Journal of The Electrochemical Society

The Electrochemical Society
Advancing solid state & electrochemical science & technology

OPEN ACCESS

Review—Solution Electrochemical Process for Fabricating Metal Oxides and the Thermodynamic Design

To cite this article: Masanobu Izaki *et al* 2021 *J. Electrochem. Soc.* **168** 112510

View the article online for updates and enhancements.

This content was downloaded from IP address 143.189.234.33 on 22/11/2021 at 22:25

Journal of The Electrochemical Society, 2021 **168** 112510

Review—Solution Electrochemical Process for Fabricating Metal Oxides and the Thermodynamic Design

Masanobu Izaki,[1,*,z] Pei Loon Khoo,[1] and Tsutomu Shinagawa[1,2]

[1]*Graduate School of Engineering, Toyohashi University of Technology, Tempaku-cho, Toyohashi-shi, Aichi 441-8580 Japan*
[2]*Electronic Materials Research Division, Morinomiya Center, Osaka Research Institute of Industrial Science and Technology, Osaka 536-8553 Japan*

Electrochemical processes in aqueous solutions are widely used for preparation of metals, alloys, composites, metal oxides and compounds. For understanding and designing an electrochemical process, it is crucial to study its soluble chemical species, potential-pH diagram, and solubility curves drawn based on thermodynamics. In this review, equilibrium electrode potentials, critical pH values, and dissolved chemical species related to the oxidation-reduction, acid-base, and ligand-exchanging reactions, in addition to the calculation based on standard Gibbs free energy are first briefly mentioned. This is followed by the description of the change in equilibrium electrode potentials of metal and metal compounds as demonstrated in the electrochemical preparation of the Cu–In–Se precursor for the $Cu(In,Ga)Se_2$ solar cell application. Additionally, the advantages and usefulness of soluble chemical species, potential-pH diagram, and solubility curves are discussed, by giving examples of direct electrodepositions of metal oxides, the chemical introduction of impurities into ZnO enabling characteristic control, the chemical bath deposition process (CBD) for Zn(S,O,OH) buffer layer in $Cu(In,Ga)Se_2$ solar cell, and lastly, the design of the electrochemical process for fabricating CuO/Cu_2O bilayers.

© 2021 The Author(s). Published on behalf of The Electrochemical Society by IOP Publishing Limited. This is an open access article distributed under the terms of the Creative Commons Attribution Non-Commercial No Derivatives 4.0 License (CC BY-NC-ND, http://creativecommons.org/licenses/by-nc-nd/4.0/), which permits non-commercial reuse, distribution, and reproduction in any medium, provided the original work is not changed in any way and is properly cited. For permission for commercial reuse, please email: permissions@ioppublishing.org. [DOI: 10.1149/1945-7111/ac371a]

Manuscript submitted July 9, 2021; revised manuscript received October 27, 2021. Published November 22, 2021.

Electrochemical processes in aqueous solutions are widely being used as electrodeposition or electroless deposition for preparing a wide variety of materials including metals such as Ni, Cu, Sn, Au, Zn, and Cr, alloys such as Ni–Fe, Sn–Pb, and Zn–Fe, and composites such as Ni–SiC, and Ni-PTFE.[1,2] Materials fabricable as films by electrochemical means are not limited to only metals but also compounds such as metal oxides and sulfides.[3–6] Lincot has summarized a roadmap of electrodepositions for inorganic semiconductors, such as Si,[7] Ge,[8] GaAs,[9] CdTe,[10,11] $CuInSe_2$, and ZnO. Switzer et al. has also reported on the direct electrodeposition of thallium oxide (Tl_2O_3) film and its heterostructure with an n-Si layer which acted as a photoanode in 1986.[12] Followingly, Izaki et al. and Lincot et al., reported the direct electrodepositions of the zinc oxide (ZnO) semiconductor films in aqueous solutions in 1996.[13–15] After that, the direct electrodepositions of various oxide semiconductors and ferromagnetic oxide films of CuO,[16–18] Cu_2O,[19–22] CeO_2,[23–26] In_2O_3,[27] Fe_3O_4,,[28–31] Fe_2O_3,[32] AgO,[33] and Ag_2O[34] have been reported. Followingly, the electrodeposition process was implemented in the preparation of precursors for photovoltaic layers of $Cu(In,Ga)Se_2$(CIGS),[35] Cu_2ZnSnS_4(CZTS),[36] and CdTe,[10,11,37] the thermoelectric layer of Bi_2Te_3,[38] as well as for precursors being used in the industrial production of CIGS solar cells.

In addition to the electrochemical process, liquid phase depositions (LPD) have also been industrially applied, such as the utilization of dehydration reaction of the metal fluoride complex in the fabrication of SiO_2 and TiO_2 films,[39–41] and the preparation of buffer layers of CdS and Zn(S,O,OH) layers in CIGS and CZTS solar cells by the chemical bath deposition (CBD) process.[42–45] Many metal complicated oxides including perovskite oxides have been synthesized by hydrothermal and solvothermal reactions.[46–48]

A common method for the formation of a metallic Cu layer on a cathode substrate by electrodeposition in an aqueous solution by the reduction of Cu^{2+} ions dissolved in an electrolyte to metal Cu is expressed by the following reaction,

$$Cu^{2+} + 2e^- \rightarrow Cu^0$$

while the oxidation (dissolution) reaction of Cu^0 to Cu^{2+} ion for the metallic Cu anode is as follows:

$$Cu^0 \rightarrow Cu^{2+} + 2e^-$$

The electron-exchanging reactions of the oxidation-reduction reactions occur respectively at the cathode and anode in the Cu electrodeposition process.

The reaction of metal cations dissolving in an aqueous solution to form oxide or hydroxide precipitation is an acid-base reaction, related to the proton exchanging reaction as can be expressed by the following example reaction in the case of Zn^{2+}:

$$Zn^{2+} + 2H_2O \rightleftarrows Zn(OH)_2 + 2H^+$$

Such acid-base reaction plays an important role in the direct electrodeposition of metal oxide films.

Many types of ligands such as ethylenediaminetetraacetic acid (EDTA), malic acid, citric acid, and lactic acid are used as additives in electrochemical preparation processes of electrodeposition and electroless deposition, allowing metals, alloys, and oxide films to form metal complexes of metal ions and ligands by the ligand-exchanging reaction.

It is usually assumed that the chemical solution reactions in aqueous solutions including acid-base and ligand-exchanging reactions reach an equilibrium state. It should be noted that the electrode reactions in practical electrodeposition processes involve applying relatively high overpotentials which deviate from equilibrium conditions. For the general information regarding the kinetics and mechanism of the electrodeposition, refer to the reported monograph.[49] However, the consideration assuming the condition of local equilibrium remains useful even in practical calculation, prediction, and design of electrochemical processes as demonstrated in the examples that will be described. Since thermodynamic calculation is a powerful tool to understand the electrochemical reactions and to design an electrochemical process to prepare desired substances based on this assumption,[50–52] further developments of electrochemical preparation processes may be yielded by thermodynamic calculation of the related reactions for realizing the preparation of metal oxides and compound films.

In this review, after a summary about the thermodynamic calculation of the oxidation-reduction reaction, acid-base reaction, and ligand-exchanging reaction, the application of the calculation regarding the drawing of the ratio of dissolved species, the potential-pH diagram for metal-water system, and the solubility curves of oxide, hydroxide, and sulfide will be discussed. The effectiveness

*Electrochemical Society Member.
[z]E-mail: m-izaki@me.tut.ac.jp

and practicality of thermodynamic calculation is then demonstrated in a variety of examples: the preparation of the $Cu(In,Ga)Se_2$ precursor by electrodeposition, the electrodeposition and chemical deposition of metal oxides of ZnO and Fe_3O_4, the chemical introduction of impurities into the ZnO film, the chemical bath deposition (CBD) of the Zn(S,O,OH) buffer layer to enhance the photovoltaic performance of the CIGS solar cell, and finally the preparation of CuO/Cu_2O bi-layers by potential-switching-deposition in a single aqueous solution.

Thermodynamic Relationships of the Oxidation-Reduction Reaction, Acid-Base Reaction, and Ligand-Exchanging Reaction

In this section, the relationships of potential (E) and pH values related to the oxidation-reduction reaction, acid-base reaction, and ligand-exchanging reaction are briefly described.

Oxidation-reduction reaction: Electron-exchanging reaction.— Oxidation-reduction reaction is a reaction with the change in the oxidation number of the metal by electron, and for example, M^{n+} is reduced to M^0 by the ne^- in the following reaction:

$$M^{n+} + ne^- \rightleftarrows M^0$$

The electrode potential (E) for this reaction is described as follows,

$$E = E^0 - \frac{RT}{nF}\log_e\frac{1}{a_{M^{n+}}}$$

where E^0, R, F, $a_{M^{n+}}$ are the standard electrode potential, gas constant, Faraday constant, and activity of the M^{n+} ion, respectively. The standard electrode potential (E^0) can be calculated by using the standard reaction Gibbs energy ($\Delta_r G^0$). Standard electrode potentials for the oxidation-reduction reaction between the metal cation and metal can be referenced from reported monographs on the electrochemistry and electroplating for pure metals, for example +0.334 V vs SHE (Standard Hydrogen Electrode) for the Cu^{2+}/Cu^0 reaction and −0.760 V vs SHE for the Zn^{2+}/Zn^0 reaction.[49]

Acid-base reaction: proton-exchanging reaction.— The acid-base reaction is a reaction accompanying the exchange of one or more protons (H^+). For example, the precipitation of a hydrated metal ion in aqueous solution as follows:

$$M^{2+} + 2H_2O \rightleftharpoons M(OH)_2 + 2H^+$$

The equilibrium constant (K) is expressed by the following equation for the reaction above:

$$K = \left(\frac{a_{M(OH)_2}a_{H^+}^2}{a_{M^{2+}}a_{H_2O}^2}\right) = \left(\frac{a_{H^+}^2}{a_{M^{2+}}}\right), \text{ where } a_{M(OH)_2} = a_{H_2O} = 1$$

Taking the logarithmic value for both sides, and using the concentration of proton $[H^+]$ as an alternative for the thermodynamic activity,

$$\log_{10}K = 2\cdot\log_{10}[H^+] - \log_{10}a_{M^{2+}}$$

And since

$$pH = -\log_{10}[H^+],$$

$$pH = \frac{1}{2}\{-\log_{10}K - \log_{10}a_{M^{2+}}\}$$

As seen above, the pH value of the acid-base reaction is a function of the activity of the dissolved metal ion, $a_{M^{2+}}$. The equilibrium constant (K) can be calculated from the standard reaction Gibbs energy. Thus, the pH value may change depending on the state of the metal dissolved in the aqueous solution, metal ion, or metal complex.

Ligand-exchange reaction.— Alkaline ammonia-complex aqueous solutions have been used for chemical bath depositions (CBD) of CdS, and Zn(O,OH,S) buffer layers installed into compound solar cells, which dissolved chemical species depend on the value of the solution pH and the concentration of the ligands to form the metal complexes.

The reaction scheme and equilibrium constant (Kc) for the formation of the ligand donor (Don) by the reaction of the ligand acceptor (Acc) and x equivalents of ligand (L) are described as follows:

$$Acc + xL \rightleftharpoons Don$$

$$Kc = \left(\frac{a_{Don}}{a_{Acc}a_L^x}\right),\ \log_{10}Kc = -x\log_{10}a_L + \log_{10}\left(\frac{a_{Don}}{a_{Acc}}\right)$$

And the reaction scheme and equilibrium constant (K) for the reaction involving both the ligand-exchanging and proton-exchanging reactions will be described in following sections.

Standard Gibbs energy of formation, equilibrium constant (K), and standard electrode potential (E^0).— The equilibrium constant (K) in the acid-base reaction and the standard electrode potential (E^0) in the oxidation-reduction reaction are respectively related to the standard reaction Gibbs energy ($\Delta_r G^0$). The relation of the chemical potential (μ_j) of the chemical substance j and total Gibbs energy (G) is expressed as follows:

$$\mu_j = \left(\frac{\partial G}{\partial n_j}\right)_{T,P} = \mu^o{}_j + RT\log_e a_j$$

where $\mu^o{}_j$ and a_j are the standard chemical potential and activity, respectively. The chemical potential is equal to the standard Gibbs energy of formation ($\Delta_f G^0$), and the values can be found in reported monographs and databases.[53,54]

The standard reaction Gibbs energy ($\Delta_r G^0$) of the following reaction:

$$aA + bB \rightleftharpoons cC + dD$$

is expressed by using chemical potentials of the chemical substances of A, B, C, and D, as follows,

$$\Delta_r G^0 = \{(c\mu^o{}_C + d\mu^o{}_D) - (a\mu^o{}_A + b\mu^o{}_B)\}.$$

The equilibrium constant (K) and the standard electrode potential (E^0) in the acid-base reaction and in the oxidation-reduction reaction each are related to the standard reaction Gibbs energy ($\Delta_r G^0$) as follows:

$$\Delta_r G^0 = -RT\log_e K$$

$$\Delta_r G^0 = -nFE^0$$

For instance, the standard electrode potential (E^0) for the reduction reactions to form metallic Zn from the metal cation of Zn^{2+} and metal complex of $Zn(NH_3)_4{}^{2+}$ can be calculated as follows. The standard chemical potentials are −147.06 kJ· mol^{-1}, −301.9 kJ· mol^{-1}, −26.5 kJ· mol^{-1}, 0 kJ· mol^{-1}, −553.59 kJ· mol^{-1}, and −237.129 kJ· mol^{-1} for Zn^{2+}, $Zn(NH_3)_4{}^{2+}$, NH_3, Zn, $Zn(OH)_2$, and H_2O, respectively.

$$Zn^{2+} + H_2 \rightleftharpoons Zn^0 + 2H^+\text{: } \Delta_r G^0$$
$$= 147.06 \text{kJ mol}^{-1},\ E^0 = -0.76\text{V vs SHE}$$

The standard reaction Gibbs free energy ($\Delta_r G^0$) is expressed for the full-cell reaction as

$$Ox + (n/2)H_2 \rightleftarrows Red + nH^+,$$

and in this review, the oxidation-reduction reactions are represented by the half-cell reaction as follows:

$$Zn^{2+} + 2e^- \rightleftarrows Zn^0$$

$$Zn(NH_3)_4^{2+} + 2e^- \rightleftarrows Zn^0 + 4NH_3: \Delta_r G^0$$
$$= 195.9 kJ\ mol^{-1},\ E^0 = -0.98V \text{ vs SHE}$$

This calculation shows that the standard electrode potential for the reduction reaction for $Zn(NH_3)_4^{2+}$ to metallic Zn shifts by approximately 0.22 V towards the negative side compared to the reduction reaction of Zn^{2+} to metallic Zn.

The equilibrium constant (K) for the formation of $Zn(OH)_2$ also changes with the formation of $Zn(NH_3)_4^{2+}$ complex as shown here:

$$Zn^{2+} + 2H_2O \rightleftarrows Zn(OH)_2 + 2H^+: \Delta_r G^0$$
$$= 67.73 kJ\ mol^{-1},\ \log_{10} K = -11.8,\ pH = 5.9 \text{ at } [Zn^{2+}] = 1 mol\ l^{-1}$$

$$Zn(NH_3)_4^{2+} + 2H_2O \rightleftarrows Zn(OH)_2 + 4NH_3 + 2H^+: \Delta_r G^0$$
$$= 116.57\ kJ\ mol^{-1},\ \log_{10} K = 20.29,\ pH = 10.1 \text{ at } [Zn(NH_3)_4^{2+}] = [NH_3]$$

Solubility product.—The solubility product constant (K_{sp}) indicates the solubility of a chemical substance and depends on the pH value and temperature. The equilibrium constant (K) for the dissolution of CdS, $CdS(s) \rightleftharpoons Cd^{2+} + S^{2-}$, for example, is expressed as follows:

$$K = \frac{a_{Cd^{2+}} \cdot a_{S^{2-}}}{a_{CdS}} = (a_{Cd^{2+}} \cdot a_{S^{2-}}),$$

where $a_{CdS} = 1$ for pure solid CdS. The solubility product (K_{sp}) for the above dissolution reaction of CdS is expressed by using the concentration of $[Cd^{2+}]$ and $[S^{2-}]$ as alternatives to the activity of $a_{Cd^{2+}}$ and $a_{S^{2-}}$, i.e., $K_{sp} = [Cd^{2+}][S^{2-}]$. The solubility products of metal complexes, oxides, hydroxides, inorganic compounds including metal salts, and sulfides can be found in reported monographs,[55] and the solubility products can be calculated based on thermodynamics aforementioned.

The activity (a) is expressed by using the activity coefficient (γ) and molar concentration (C) as follows; $a = \gamma \cdot C$, and some values of the activity coefficient can be found in reported monograph.[53] Molar concentration (C) will be used as the alternative to activity (a) in calculations in the following sections. It should be noted that the use of molar concentration may introduce uncertainties in the calculation results, which degree is dependent on the molar concentration of the dissolved species. However, electrochemical predictions and designs with such calculations are possible and useful, as will be demonstrated in examples in this review.

Application of the Thermodynamics to the Design and Approval of Electrochemical Processes

Preparation of precursors of compound semiconductor layers for solar cells by solution electrochemical reactions.—Many research works on the electrochemical preparation of precursors have been carried out for compounds such as $CuInSe_2$,[35] Cu_2ZnSnS_4,[36] CdTe,[10,11] and Bi_2Te_3.[38] These compound semiconductors installed into solar cells and thermoelectric devices are prepared with methods that generally include firstly heating their precursors in vacuum or in a controlled atmosphere. The process to prepare these compound semiconductor layers can be commonly specified into two types, i) annealing of layered structure composing all metal element layers, or ii) annealing of the alloy layer containing all elements.

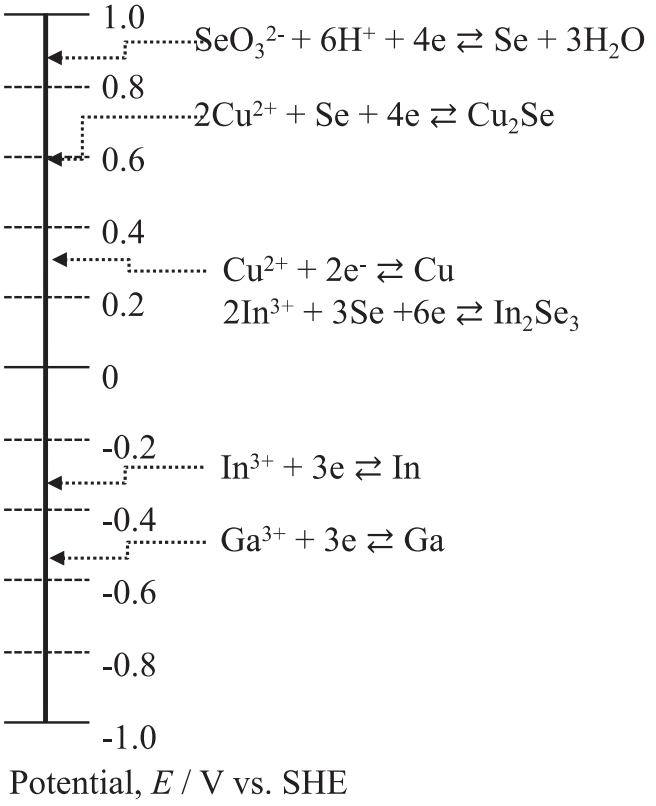

Figure 1. Standard equilibrium electrode potentials for oxidation-reduction reaction for Cu, In, Se, Cu_2Se, and In_2Se_3.

In 2004, Takei et al. reported the preparation of $CuInSe_2$(CIS) solar cells by a three-steps-process which utilized electrodeposition as follows. The first step was the electrodeposition of a Cu layer on a Mo/soda-lime-glass substrate in a Cu-sulfate aqueous solution, followed by the electrodeposition of an In layer on the Cu layer in an In-methanesulfonic aqueous solution to fabricate a Cu/In bilayer. The $CuInSe_2$ layer was then prepared by subsequently heating the Cu/In bilayer precursor in H_2Se atmosphere. A power conversion efficiency (PCE) of 9.4% was reported for the resultant $CuInSe_2$(CIS) solar cell.[56] Ahmed et al. reported a Cu_2ZnSnS_4 (CZTS) solar cell with a PCE of 7.4% which was fabricated by the electrodeposition of Cu/Zn/Sn layered precursors followed by heating in S atmosphere in 2012.[36] The rationales for the use of layered precursors to prepare compound semiconductors of $CuInSe_2$(CIS) and Cu_2ZnSnS_4 (CZTS) layers are as follows. The first was to establish the electrodeposition technique to prepare the single metal layers of Cu, In, and Zn, and the second was due to the difficulty of forming alloy layers containing these elements owing to the differences in standard electrode potentials. Figure 1 shows the standard electrode potential for the following reactions to deposit Cu, In, and Se metals.

$$Cu^{2+} + 2e^- \rightleftarrows Cu: E = 0.337 + 0.0295 \cdot \log_{10}[Cu^{2+}] (V \text{ vs SHE})$$

$$In^{3+} + 3e^- \rightleftarrows In: E = -0.342 + 0.0197 \cdot \log_{10}[In^{3+}] (V \text{ vs SHE})$$

$$SeO_3^{2-} + 6H^+ + 4e^- \rightleftarrows Se + 3H_2O:$$
$$E = 0.875 - 0.0886pH$$
$$-0.0148 \cdot \log_{10}[SeO_3^{2-}] (V \text{ vs SHE})$$

The equilibrium electrode potential (V vs SHE) at $[Cu^{2+}] = [In^{3+}] = [SeO_3^{2-}] = 1\ mol\ l^{-1}$ was 0.337 V for Cu^{2+}/Cu, −0.342 V vs SHE for In^{3+}/In, and 0.875 − 0.0886 pH (V vs SHE) for SeO_3^{2-}/Se systems, and the difference between the equilibrium electrode potentials for the In^{3+}/In^0 and Cu^{2+}/Cu^0 system is at a significant value of 0.67 V vs SHE. In an aqueous solution containing both the Cu^{2+} and In^{3+} ions, only the metallic Cu is deposited at potentials ranging from 0.337 V vs SHE to −0.342 V vs SHE, while the Cu-In alloy can only be deposited at potentials more negative than −0.342 V vs SHE, which composition varies with the deposition potential. While at electrodeposition potentials in the limiting current density region, it is possible for a Cu–In alloy layer to be deposited with an almost constant composition, but the current efficiency will be drastically reduced due to the evolution of hydrogen gas.

Lincot et al. reported the possibility of electrodepositing such alloys by reducing the difference in standard electrode potentials from 0.67 V vs SHE to 0.27 V vs SHE by considering the formation of In_2Se_3 and Cu_2Se in aqueous solutions containing metal cations of Cu^{2+}/In^{3+} and SeO_3^{2-} as follows:

$$2In^{3+} + 3Se + 6e^- \rightleftarrows In_2Se_3\text{: } E^0 = 0.33V \text{ vs SHE}$$

$$2Cu^{2+} + Se + 4e^- \rightleftarrows Cu_2Se\text{: } E^0 = 0.60V \text{ vs SHE}$$

As such, $CuInSe_2$ (CIS) solar cells could be successfully fabricated using a Cu–In–Se precursor prepared by electrodeposition in an aqueous solution containing Cu^{2+}, In^{3+}, and SeO_3^{2-} ions.[57,58] Also, Aksu et al. reported the fabrication of a Cu(In,Ga)Se_2 (CIGS) solar cell by heating an In–Se/Ga–Se/Cu-layered precursor prepared by electrodeposition in an aqueous solution containing Cu−, In−, and Ga-complexes.[59] Additionally, Murase et al. successfully prepared a CdTe layer by electrodeposition from an aqueous solution containing an alkaline metal-ammonia complex.[37] These methods involve thermodynamic calculation including the reactions of metal complexes, which will be discussed in detail in the following section.

Electrodeposition of oxide layers by electrochemical reactions.—Figure 2 shows the potential-pH diagram for a Zn-water system and the solubility curve for ZnO. In the potential-pH diagram, the vertical and horizontal axes are the electrode potential relating to the oxidation-reduction reaction and the pH value relating to the acid-base reaction, respectively, and the stable regions of cation, metal, and oxide (hydroxides) are two-dimensionally demonstrated (Fig. 2A). Since M. Pourbaix from the University of Brussels summarized an atlas of electrochemical equilibria in aqueous solutions and derived the potential-pH diagram (better known as the Pourbaix diagram) in 1963, such diagrams have been widely used to understand corrosions and electrodepositions.[51]

The two dotted lines of (a) and (b) show the reactions for the generation of H_2 and O_2 gases, which reactions and equilibrium electrode potentials are shown as follows:

(a) $H^+ + e^- \leftrightarrows \frac{1}{2}H_2$: $E = 0.000 - 0.0591pH$(V vs SHE)
(b) $O_2 + 4H^+ + 4e^- \leftrightarrows 2H_2O$: $E = 1.228 - 0.0591pH$(V vs SHE)

The thermodynamically stable regions of the zinc species, including Zn^{2+}(aq), ZnO(s), Zn(s), and ZnO_2^{2-}(aq), are represented in the potential-pH diagram for the Zn-water system, and the reactions and related equilibrium electrode potentials and pH values are as follows:

$$Zn^{2+} + 2e^- \rightleftharpoons Zn,\ E = -0.763 + 0.0295 \cdot \log_{10}[Zn^{2+}] \text{(V vs SHE)}$$

$$ZnO + 2H^+ + 2e^- \rightleftharpoons Zn + H_2O,\ E = -0.439 - 0.591pH \text{(V vs SHE)}$$

$$Zn^{2+} + H_2O \rightleftharpoons ZnO + 2H^+,\ \log_{10}[Zn^{2+}] = 10.96 - 2pH$$

$$ZnO + H_2O \rightleftharpoons ZnO_2^{2-} + 2H^+,\ \log_{10}[ZnO_2^{2-}] = -29.78 + 2pH$$

Excluding reactions (a), and (b), the vertical, horizontal, and diagonal lines correspond to the above reactions and were calculated and drawn under the condition of $[Zn^{2+}] = [ZnO_2^{2-}] = 10^{-2}\ mol\ l^{-1}$ and 298 K. As seen in Fig. 2A, the ZnO(s) region is in a relatively high pH area, while the Zn(s) region is located at a more negative potential side compared to the Zn^{2+}(aq) region. This means that a metal Zn layer can be deposited by cathodic polarization at potentials more negative than −0.822 V vs SHE on a cathode substrate immersed into an aqueous solution of dissolved zinc salts, and this electrodeposition process can be yielded by shifting the electrode potential negatively from the stable Zn^{2+} region downwards crossing the horizontal line for the Zn^{2+}/Zn reaction. The potential and pH values related to the oxidation-reduction and acid-base reactions depends on the metal complex species, and industrially employed aqueous solutions used for electrodeposition and electroless deposition often contain organic and inorganic ligands in addition to metal salts. Figure 2B shows the solubility curve of ZnO, which is the dependence of ZnO solubility on the pH value. ZnO showed a minimum solubility at approximately pH 10 which value increases by either increasing or decreasing the pH. When the total Zn concentration is lower than the solubility curve, no precipitate and the dissolved Zn species exist in the aqueous solution, whereas when the total Zn concentration is higher than the solubility curve, part of the Zn ion excess precipitate as ZnO due to supersaturation. ZnO precipitation may occur throughout the solution if the pH value of the entire aqueous solution is raised. Likewise, the formation of ZnO layer on a substrate can be anticipated if the local pH value in the vicinity of the substrate is raised. Izaki et al. and Lincot et al. reported the first direct electrodepositions of ZnO layers by using the reduction reaction of nitrate (NO_3^-) ions and dissolved molecular oxygens (O_2) to elevate the local pH value in the vicinity of the substrate,[13,14] which can be shown as:

$$NO_3^- + H_2O + 2e^- \rightleftharpoons NO_2^- + 2OH^-,$$
$$\Delta_r G^0 = -0.819\ kJ \cdot mol^{-1},\ E^0 = 0.004\ V \text{ vs SHE}$$

$$O_2 + 2H_2O + 4e^- \rightleftharpoons 4OH^-,$$
$$\Delta_r G^0 = -85.91\ kJ \cdot mol^{-1},\ E^0 = 0.40\ V \text{ vs SHE.}$$

The pH value in the direct proximity of the substrate is increased with the generation of the OH^- ions, and as a result a ZnO layer is precipitated and deposited on the substrate. Before and after the precipitation, the oxidation number of Zn is constant at +2, while the nitrate ions (NO_3^-) and dissolved molecular oxygens (O_2) are reduced to nitrite ions (NO_2^-) and OH^-. Since the standard reaction Gibbs energy ($\Delta_r G^0$) is −1.6 kJ mol^{-1} for the following dehydration reaction from $Zn(OH)_2$ to ZnO, this exergonic ZnO formation reaction proceeds spontaneously under the equilibrium state:

$$Zn(OH)_2 \rightleftharpoons ZnO + H_2O$$

Lincot et al. also reported the dissolved species, solubility curves, and deposition mechanism by considering the Zn-chlorine complex based on thermodynamics.[60] The equilibrium electrode potential (E) for the metal Zn electrodeposition is estimated to be −0.763 V vs SHE at $[Zn^{2+}] = 1 mol\ l^{-1}$.

$$Zn^{2+} + 2e^- \rightleftharpoons Zn,\ E = -0.7 \cdot 63 + 0.0295 \cdot \log_{10}[Zn^{2+}] \text{(V vs SHE)}$$

This indicates that the metal Zn component can be deposited simultaneously with ZnO at potentials more negative than −0.763 V vs SHE, which is in the Zn stable region as seen in the

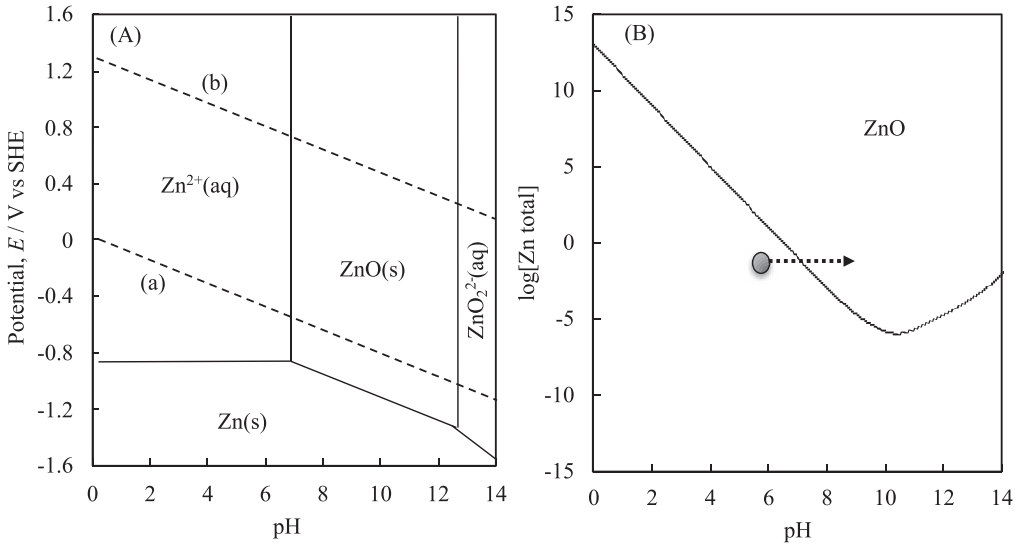

Figure 2. Potential-pH diagram (A) and solubility curve (B) of ZnO for the Zn-water system at $[Zn^{2+}]=10^{-2}$ mol l^{-1} and T = 298 K. (a) $H_2 \leftrightarrows 2H^+ + 2e^-$, $E^0 = 0 + 0.0591$ pH (V vs SHE), (b) $2H_2O \leftrightarrows O_2 + 4H + + 4e^-$, $E^0 = 1.228–0.0591$ pH (V vs SHE).

potential-pH diagram for the Zn-water system. Single-phase ZnO can be obtained at electrode potentials ranging from −0.763 V vs SHE up to 0.0 V vs SHE for the nitrate ion system, or up to 0.40 V vs SHE for the dissolved molecular oxygen system.

In addition to the formation of ZnO, direct crystal growth of layered zinc hydroxides (LZHs) has also been reported under cathodic polarization of aqueous solution containing $Zn(NO_3)_2$. By using a layer-by-layer (LbL)-coated ITO substrate, electrodeposition with controlled crystal orientation of LZHs is also possible.[61,62] Layered zinc hydroxides have a chemical formula of $Zn_x(OH)_{2x-my}(A^{m-})_y \cdot nH_2O$, ($A^{m-}$ = Cl^-, NO_3^-, SO_4^{2-}, and CO_3^{2-}), and some of these LZHs generate nanoporous ZnO when thermally decomposed while maintaining the original crystal orientation. Taking advantage of this feature, highly <0001>-oriented nanoporous ZnO films could be obtained by thermal decomposition of the oriented LZHs prepared electrochemically.[62,63]

A plausible electrodeposition reaction of LZHs is shown below using layered zinc hydroxy nitrate ($Zn_5(NO_3)_2(OH)_8 \cdot 2H_2O$; Z5HN) as an example:

$$NO_3^- + H_2O + 2e^- \rightleftharpoons 2OH^- + NO_2^-$$

$$5Zn^{2+} + 2NO_3^- + 8OH^- + 2H_2O \rightleftharpoons Zn_5(NO_3)_2(OH)_8 \times 2H_2O,\ \log_{10}K = 68.3$$

By using the standard Gibbs energy of the formation for Z5HN reported in past literature,[63] which is −3,079.89 kJ· mol^{-1}, the equilibrium constant K, is calculated to be $\log_{10}K = 68.3$. From this value, the boundary (critical) pH of the stable region of Zn^{2+}(aq) and Z5HN(s) can be estimated. In Fig. 3, the critical pH value as a function of the logarithm of the $Zn(NO_3)_2$ concentration is plotted in comparison with that of $Zn(OH)_2$. Both the critical pH values descend linearly from 8–9 to 5–6 with increasing $Zn(NO_3)_2$ concentration, though the slopes of the two lines are different. When the $Zn(NO_3)_2$ concentration is 0.1 mol l^{-1} or more, the critical pH value of Z5HN becomes smaller than that of $Zn(OH)_2$, suggesting that Z5HN is preferentially deposited compared to $Zn(OH)_2$ at higher concentrations. In fact, the deposits obtained experimentally by electrodeposition from $Zn(NO_3)_2$ changed from ZnO to Z5HN with increasing $Zn(NO_3)_2$ concentration, which was consistent with the thermodynamic prediction.[62,64]

Figure 4 shows the scanning electron microscopy (SEM) image of a vertical-ZnO-nanowire layer prepared by a heteroepitaxial electrodeposition method. This ZnO layer with vertical nanowires

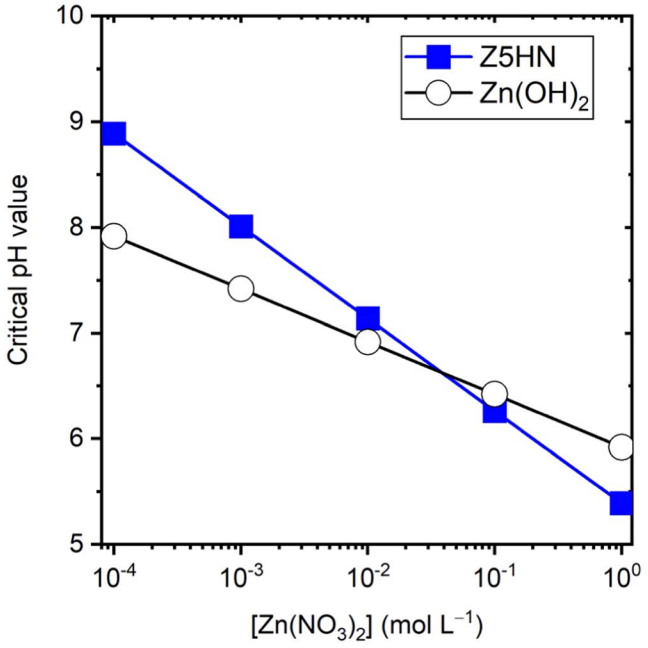

Figure 3. Plot of the critical pH value of $Zn^{2+} \leftrightarrow$ Z5HN and $Zn^{2+} \leftrightarrow Zn(OH)_2$ as a function of the concentration of $Zn(NO_3)_2$.

possessed a ⟨0001⟩-out-of-plane orientation, and ultraviolet light emission was confirmed under the irradiation of synchrotron X-ray radiation originating from the recombination of excitons at room temperature.[65–68] The nanowire-ZnO is a realistic candidate for the next-generation scintillator materials, and a spatial resolution of 2 μm for synchrotron X-ray radiation was reported for the electrochemically-prepared ZnO vertical nanowires scintillator.[69] Water and hydroxides were not detected when investigated by Fourier-transform infrared spectroscopy (FT-IR), X-ray photoelectron spectroscopy, and X-ray absorption fine structure (XAFS) analyses, and the pristine ZnO layer and nanowires displayed decent semiconductor qualities without the need of any post-deposition processes such as heating.[64] As aforementioned, the standard reaction Gibbs energy ($\Delta_r G^0$) of the dehydration reaction from $Zn(OH)_2$ to ZnO is of a negative value, i.e. exergonic, resulting in spontaneous reaction and thus a direct electrodeposition of ZnO. The nature of the $\Delta_r G^0$

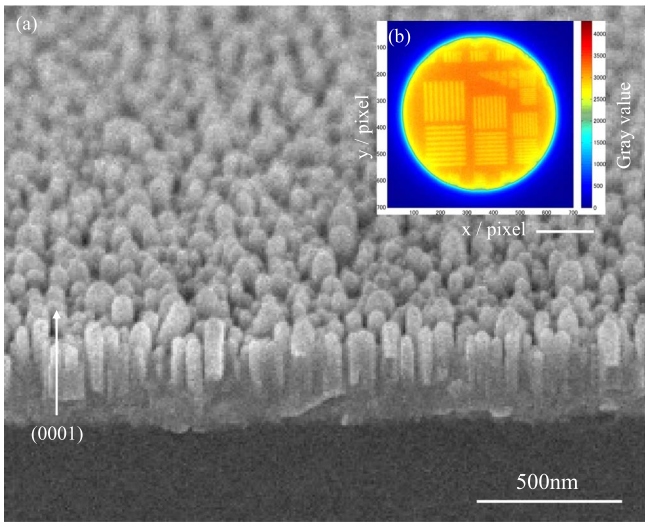

Figure 4. FE-SEM image of the electrodeposited ⟨0001⟩-ZnO-vertical nanowires (a) and the special resolution image by Synchrotron X-ray radiation(b).

value of a dehydration reaction, whether negative or positive, strongly affects the possibility of its metal oxide formation by electrodeposition. Some metal oxides aside ZnO, such as Fe_3O_4 and CeO_2 can also be directly deposited due to the negative $\Delta_r G^0$ values for their dehydration reactions, while others with positive values stop short at the formation of metal hydroxides such as $In(OH)_3$. Generally, when the stable region of a metal oxide and/or hydroxide is located at pH values higher than its metal cation region in the potential-pH diagram, metal oxide and/or hydroxide can be prepared directly by raising the local pH value by using the reduction of nitrate ions (NO_3^-) and dissolved molecular oxygens (O_2). This strategy suggests the possibility to prepare other metal oxides and hydroxides using this method, such as SiO_2, TiO_2, $Tb(OH)_3$, and $In(OH)_3$.

In the electrochemical deposition of metal oxides using nitrate ions, the oxides are induced by the reduction reaction of the nitrate ions and not metal cations. Thus, when a chemical substance possessing a standard electrode potential more negative than for the nitrate reduction reaction is simultaneously present in an aqueous solution used for an oxide electrodeposition, it is possible for the metal oxide or hydroxide layer to be chemically deposited without any external power supply, because such chemical substances can act as reducing agents to the nitrate ions. As an example, the oxidation reaction, standard reaction Gibbs energy, and standard electrode potential for borohydride ions are shown as follows, which metal oxides could be prepared by adding the borohydride ion into the aqueous solution containing the metal cations and nitrate ions.

$$BO_2^- + 6H_2O + 8e^- \rightleftarrows BH_4^- + 8OH^-:$$
$$\Delta_r G^0 = -958.062\ \text{kJ·mol}^{-1},\ E^0 = -1.24\ V\ \text{vs SHE}$$

Since the critical equilibrium pH value for the acid-base reactions of the oxide formation depends on the metal element, boron compounds of dimethylamine borane (DMAB, $(CH_3)_2NHBH_3$), and trimethylamine borane (TMAB) are used instead for the chemical deposition of ZnO,[70] Fe_3O_4,[29] and CeO_2.[23] The oxidation reaction of DMAB is shown as follows:[71,72]

$$(CH_3)_2NHBH_3 + H_2O \rightleftarrows HBO_2 + (CH_3)_2NH_2^+ + 5H^+ + 6e^-$$

As mentioned, metal oxides whose stable region is located at higher pH values of the metal cation stable region in the potential-pH diagram can be prepared by increasing the local pH value using the cathodic reaction of nitrate ions and/or dissolved molecular oxygens. On the contrary, when the stable region of oxides is located at lower pH values than that of their metal ions, the oxides or hydroxides can be deposited by decreasing the local pH value using the anodic reaction of water, which gives H^+, as demonstrated for the anodic deposition of tungsten oxide hydrate.[73,74] However, when the reduction potential of metal ions is close to the reduction potential of nitrate ions and dissolved molecular oxygens, a different approach is necessary. A strategy for overcoming this obstacle is the formation of dissolved metal complexes in which the stable region is surrounded by metal oxides, as demonstrated by the direct electrodeposition of CuO and Ag_2O.[17,34]

Chemical introduction of impurities into ZnO to control the characteristics.—Zinc oxide (ZnO) is an n-type semiconductor with the bandgap energy of 3.3 eV and exciton binding energy of 59 meV and has been widely employed as transparent conductive window-layers for solar cells and liquid crystal displays, high-frequency filters, and piezo-electric devices. The ZnO layer used for the electronics application has been mainly prepared by vacuum processes such as sputtering, and several types of impurities which act as donors and acceptors are introduced to control the electrical and optical characteristics demanded in the applications. Here the electrochemical introductions of impurities into ZnO are discussed. While trivalent elements such as Al^{3+}, Ga^{3+}, and In^{3+} act as donors in ZnO semiconductors and are generally introduced to reduce the electrical resistivity in applications of transparent conductive window-layers, chlorine impurity (Cl^-) has also been reported to induce decrease of resistivity of the ZnO layer.[75–77]

The formation reactions of the ZnO are described as follows:

$$NO_3^- + H_2O + 2e^- \rightleftarrows NO_2^- + 2OH^-,$$
$$\Delta_r G^0 = -0.819\ \text{kJ·mol}^{-1},\ E^0 = 0.004\ \text{V vs SHE}$$

$$Zn^{2+} + H_2O \rightleftarrows ZnO + 2H^+:\ \text{pH} = 5.48 - 1/2\log_{10}[Zn^{2+}]$$

while the reactions and equilibrium pH values for the formation of metals and oxides of Al, Ga, and In elements are described as follows:

$$Al^{3+} + 3e^- \rightleftarrows Al:\ E^0 = -1.663\text{V vs SHE}$$

$$2Al^{3+} + 3H_2O \rightleftarrows Al_2O_3 + 6H^+:\ \text{pH} = 1.9 - 1/3\cdot\log_{10}[Al^{3+}]$$

$$Ga^{3+} + 3e^- \rightleftarrows Ga:\ E^0 = -0.529\text{V vs SHE}$$

$$2Ga^{3+} + 3H_2O \rightleftarrows Ga_2O_3 + 6H^+:\ \text{pH} = 0.74 - 1/3\cdot\log_{10}[Ga^{3+}]$$

$$In^{3+} + 3e^- \rightleftarrows In:\ E^0 = -0.34\ \text{V vs SHE}$$

$$2In^{3+} + 3H_2O \rightleftarrows In_2O_3 + 6H^+:\ \text{pH} = 2.57 - 1/3\cdot\log_{10}[In^{3+}]$$

Since the standard electrode potentials (E^0) for the oxidation/reduction reactions of Al^{3+}/Al, Ga^{3+}/Ga, and In^{3+}/In are negative than that for the NO_3^-/NO_2^- reaction, metal oxides or hydroxides can be prepared by the reduction reaction of nitrate ion. The equilibrium pH values for Al^{3+}/Al_2O_3, Ga^{3+}/Ga_2O, and In^{3+}/In_2O_3 at $[Al^{3+}] = [Ga^{3+}] = [In^{3+}] = 1\ \text{mol l}^{-1}$ are lower than that for the Zn^{2+}/ZnO, and the pH value for the mixed aqueous solution is governed by the reaction with lower critical pH value, according to the equation of $\text{pH} = -\log_{10}[H^+]$. The aqueous solution containing both Zn^{2+} and In^{3+} ions showed a pH value of 2.57 owing to the In^{3+}/In_2O_3 reaction at $[In^{3+}] = 1\ \text{mol l}^{-1}$. It is predicted that only $In(OH)_3$ will be deposited at pH values ranging from 2.57 to 5.48 for the Zn^{2+}/ZnO reaction at $[Zn^{2+}] = 1\ \text{mol l}^{-1}$, while a mixture of ZnO and $In(OH)_3$ will be deposited at pH values higher than 5.48 in a mixed aqueous solution containing the Zn^{2+},

In^{3+}, and NO_3^-. A decrease in In^{3+} concentration to 6.15×10^{-5} mol l^{-1} is needed at $[Zn^{2+}] = 0.05$ mol l^{-1} to achieve the critical pH value for both the Zn^{2+}/ZnO and In^{3+}/In_2O_3 reactions in the mixed aqueous solution, indicating that the electrochemical deposition of the Zn–In–O cannot be easily achieved. Thus, it can be concluded that it is difficult to electrochemically deposit ZnO semiconductors containing trace amount of In^{3+}, Al^{3+}, and Ga^{3+} in mixed aqueous solutions, for the reasons aforementioned.

While for a Zn–Ce–O layer, since the critical pH value for the Ce^{3+}/Ce_2O_3 is close to that for the Zn^{2+}/ZnO reaction as follows, it can be obtained from a mixed aqueous solution, as already reported.[76]

$$2Ce^{3+} + 3H_2O \rightleftarrows Ce_2O_3 + 6H^+: \text{pH} = 7.381/3 \cdot \log_{10}[Ce^{3+}]$$

Lincot et al. reported that a Cl:ZnO layer can be deposited by raising the local pH value according to the solubility curves drawn by considering the Zn–Cl complex, and that Cl impurities act as donors in the ZnO semiconductor.[77,78] The chemically prepared ZnO layers also contained trace amount of B^{3+} impurity originating from the DMAB used as the reducing agent, and the introduced B^{3+} impurities also contributed to the decrease in resistivity by acting as donors.[79,80]

Izaki, et al. reported the chemical introduction of In^{3+} and $Fe^{2+,3+}$ impurities into a ZnO layer by immersing the ZnO layer in an aqueous solution containing the impurity ions.[81,82] The exchanging reaction and the standard reaction Gibbs energy are described as follows;

$$3ZnO + 2In^{3+} \rightleftarrows In_2O_3 + 3Zn^{2+}: \Delta_r G^0 = -121.7 \text{ kJ} \cdot \text{mol}^{-1}$$

$$4ZnO + Fe^{2+} + 2Fe^{3+} \rightleftarrows Fe_3O_4 + 4Zn^{2+}: \Delta_r G^0 = -247.8 \text{ kJ} \cdot \text{mol}^{-1}$$

Since the standard reaction Gibbs energy for both reactions are negative, In^{3+} and $Fe^{2+,3+}$ impurities can be introduced into the ZnO layer by these exchanging reactions occurring spontaneously. These reactions took place at the interface between the ZnO layer and the impurity-containing aqueous solution, where the introduced impurities diffused into the ZnO layer. A concentration gradient was present initially for the impurities, with the highest concentration at the surface of the ZnO layer, which distributed throughout the ZnO layer after enough time had passed. The ZnO layer without impurities showed a resistivity in the order of 10^{-3} Ω cm, which increased to 1.71 Ω cm when exposed to an atmosphere of 353 K and 95% in humidity for 24 h. The In:ZnO layer, however, kept a low resistivity of 8.4×10^{-4} Ω cm and exhibited high stability even when exposed to the same condition due to its In-rich oxide layer near the surface. The ZnO layer without impurities did not reveal any ferromagnetism, but a Fe:ZnO layer prepared by this exchanging reaction method possessed ferromagnetism at room temperature. As demonstrated here, the In:ZnO and Fe:ZnO layers were not realized by simultaneous electrodeposition, but by exchanging reactions. This highlights the versatility of effective utilization of the standard reaction Gibbs energy in the preparation of various types of impurity-incorporated oxide layers achievable by simultaneous deposition or exchanging reactions, depending on the desired impurities.

Chemical bath deposition (CBD) of Zn(S,O,OH) layer and the enhancement of the performance of Cu(In,Ga)Se_2 solar cells.— Consideration for the effects of the metal complexes is unnecessary to understand the deposition mechanism in an electrodeposition of metal oxides via the reduction reaction of nitrate ions because metal ions exist as hydrate ions in the aqueous solution. Metal complexes formed by adding inorganic and organic ligands, however, are widely applied in industrial applications of electroplating, electroless plating, and especially in the chemical bath deposition (CBD) processes used for the preparation of the CdS, and Zn(S,O,OH) buffer layers installed into Cu(In,Ga)Se_2 solar cells. Metal sulfides and sulfide oxides such as Cu_xS,[83] Cu(O,S),[84] ZnS,[85] ZnSe,[86] and $In_x(OH)_ySz$[87] can be prepared by CBD using metal-complex species, such as the metal-NH_3 complex. However, it is important to note that the formation of metal complexes affects not only the standard electrode potentials and equilibrium pH values related to the oxidation-reduction and acid-base reactions, but also the profiles of the potential-pH diagram and solubility curve.[88,89]

The aqueous solution used for the CBD process contains zinc acetate and zinc nitrate as the Zn salts, NH_3 as the ligand, and thiourea as the sulfur source. There are some dissolved species of Zn^{2+}, $Zn(OH)^+$, $Zn(OH)_2$, $Zn(OH)_3^-$, and $Zn(OH)_4^{2-}$ in the Zn-water system, and by adding ammonia (NH_3), it induces the formation of additional dissolved species of Zn-NH_3 complexes such as $ZnNH_3^{2+}$, $Zn(NH_3)_2^{2+}$, $Zn(NH_3)_3^{2+}$, and $Zn(NH_3)_4^{2+}$, with the formation ratio depending on pH value and NH_3 concentration. Figure 5 shows the formation ratio of the dissolved Zn(II) species and Zn-NH_3 complex species as a function of the pH value. The relationships between the formation ratio and pH value were calculated and drawn by the following steps, using the stability constants (K) published in monographs and databases.[90] Stability constants can be calculated from the chemical potential for each

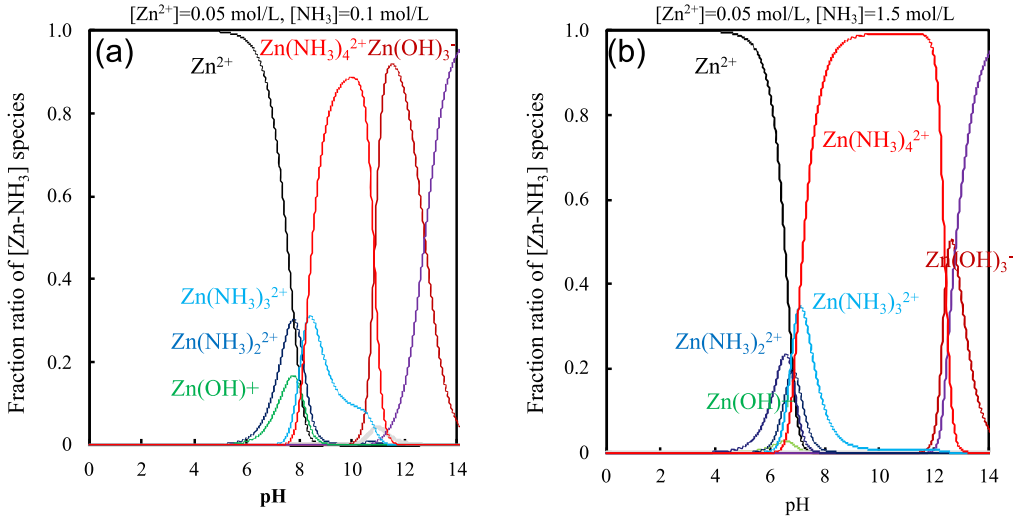

Figure 5. Effects of the pH value and NH_3 concentration on the ratio of dissolved species for Zn-NH_3-water system at 298 K.

chemical substances of metal cation, metal-complex, and ligand using the equation $\Delta_r G^0 = -RT \log_e K$.

$$Zn^{2+} + NH_3 \rightleftharpoons Zn(NH_3)^{2+} (K_1)$$

$$K_1 = [Zn(NH_3)^{2+}]/([Zn^{2+}][NH_3]),\ \log_{10} K_1 = 2.38$$

$$[Zn(NH_3)^{2+}] = K_1[Zn^{2+}][NH_3]$$

$$Zn(NH_3)^{2+} + NH_3 \rightleftharpoons Zn(NH_3)_2^{2+} (K_2)$$

$$K_2 = [Zn(NH_3)_2^{2+}]/([Zn(NH_3)^{2+}][NH_3]),\ \log_{10} K_2 = 2.5$$

$$[Zn(NH_3)_2^{2+}] = K_2[Zn(NH_3)^{2+}][NH_3] = K_1K_2[Zn^{2+}][NH_3]^2$$

$$Zn(NH_3)_2^{2+} + NH_3 \rightleftharpoons Zn(NH_3)_3^{2+} (K_3)$$

$$\log_{10} K_3 = 2.55$$

$$[Zn(NH_3)_3^{2+}] = K_3[Zn(NH_3)_2^{2+}][NH_3] = K_1K_2K_3[Zn^{2+}][NH_3]^3$$

$$Zn(NH_3)_3^{2+} + NH_3 \rightleftharpoons Zn(NH_3)_4^{2+} (K_4)$$

$$\log_{10} K_4 = 2.22$$

$$[Zn(NH_3)_4^{2+}] = K_4[Zn(NH_3)_3^{2+}][NH_3] = K_1K_2K_3K_4[Zn^{2+}][NH_3]^4$$

$$\begin{aligned}[Zn_{total}] &= [Zn^{2+}] + [Zn(NH_3)^{2+}] + [Zn(NH_3)_2^{2+}] \\ &+ [Zn(NH_3)_3^{2+}] + [Zn(NH_3)_4^{2+}] \\ &= [Zn^{2+}](1 + K_1[NH_3] + K_1K_2[NH_3]^2 \\ &+ K_1K_2K_3[NH_3]^3 + K_1K_2K_3K_4[NH_3]^4)\end{aligned}$$

The ratio of the dissolved species, for example Zn^{2+}, can be calculated by the following equation, and the ratio is a function of the NH_3 concentration.

$$\frac{[Zn^{2+}]}{[Zn_{total}]} = 1/(1 + K_1[NH_3] + K_1K_2[NH_3]^2 + K_1K_2K_3[NH_3]^3 + K_1K_2K_3K_4[NH_3]^4)$$

The dissolved Zn(II) species in the aqueous solution exist as hydrate Zn^{2+} ions at very low NH_3 concentrations, and the conformation of the Zn-NH_3 complex changed from $Zn(NH_3)^{2+}$, $Zn(NH_3)_2{}^{2+}$, $Zn(NH_3)_3{}^{2+}$, and $Zn(NH_3)_4{}^{2+}$with increase in NH_3 concentration to $\log_{10}[NH_3]= 0$, that is $[NH_3] = 1$ mol l^{-1}. The reactions to form a solid-state $Zn(OH)_2$ from these Zn-NH_3 complexes can be described as follows;

$$Zn(OH)_2 + 2H^+ + NH_3 \rightleftharpoons ZnNH_3^{2+} + 2H_2O\ (K_{N1})$$

$$\log_{10}[ZnNH_3^{2+}] = \log_{10} K_{N1} + \log_{10}[NH_3] - 2pH,\ K_{N1} = 6.5 \times 10^{13}$$

$$Zn(OH)_2 + 2H^+ + 2NH_3 \rightleftharpoons Zn(NH_3)_2^{2+} + 2H_2O,\ (KN_2)$$

$$\log_{10}[Zn(NH_3)_2^{2+}] = \log_{10} K_{N2} + 2\log_{10}[NH_3] - 2pH,\ K_{N2} = 1.27 \times 10^{16}$$

$$Zn(OH)_2 + 2H^+ + 3NH_3 \rightleftharpoons Zn(NH_3)_3^{2+} + 2H_2O,\ (K_{N3})$$

$$\log_{10} g[Zn(NH_3)_3^{2+}] = \log_{10} K_{N3} + 3\log_{10} g[NH_3] - 2pH,\ K_{N3} = 2.91 \times 10^{18}$$

$$Zn(OH)_2 + 2H^+ + 4NH_3 \rightleftharpoons Zn(NH_3)_4^{2+} + 2H_2O,\ (K_{N4})$$

$$\log_{10}[Zn(NH_3)_4^{2+}] = \log_{10} K_{N4} + 4\log_{10}[NH_3] - 2pH,\ K_{N4} = 3.12 \times 10^{20}$$

The equilibrium reaction and equilibrium constant for NH_3 are as follows:

$$NH_4{}^+ \rightleftarrows NH_3 + H^+,\ K_{AN} = 5.62 \times 10^{-10}$$

Zinc hydroxide ($Zn(OH)_2$) can also be dissolved as $Zn(OH)^+$, $Zn(OH)_2{}^0$, $Zn(OH)_3{}^-$, and $Zn(OH)_4{}^{2-}$ by the following reactions:

$$Zn(OH)_2 + H^+ \rightleftharpoons Zn(OH)^+ + H_2O\ (K_{O1})$$

$$\log_{10}[Zn(OH)^+] = \log_{10} K_{O1} - pH,\ K_{O1} = 6.48 \times 10^3$$

$$Zn(OH)_2 \rightleftharpoons Zn(OH)_2^0 (K_{O_2})$$

$$\log_{10}[Zn(OH)_2^0] = \log_{10} K_{O_2},\ K_{O_2} = 5.23 \times 10^{-6}$$

$$Zn(OH)_2 + H_2O \rightleftharpoons Zn(OH)_3^- + H^+ (K_{O3})$$

$$\log_{10}[Zn(OH)_3^-] = \log_{10} K_{O3} + pH,\ K_{O3} = 1.68 \times 10^{-17}$$

$$Zn(OH)_2 + 2H_2O \rightleftharpoons Zn(OH)_4^{-2} + 2H^+ (K_{O4})$$

$$\log_{10}[Zn(OH)_4^{-2}] = \log_{10} K_{O4} + 2pH,\ K_{O4} = 2.71 \times 10^{-30}$$

In this case, the total concentration of dissolved Zn(II) species is expressed as follows:

$$\begin{aligned}[Zn_{total}] &= [Zn^{2+}] + [Zn(OH)^+] + [Zn(OH)_2^0] + [Zn(OH)_3^-] \\ &+ [Zn(OH)_4^{2-}] + [Zn(NH_3)^{2+}] + [Zn(NH_3)_2^{2+}] \\ &+ [Zn(NH_3)_3^{2+}] + [Zn(NH_3)_4^{2+}]\end{aligned}$$

The formation ratio of dissolved species, for example $[Zn(NH_3)_4{}^{2+}]$, can be obtained by calculating $[Zn(NH_3)_4{}^{2+}]/[Zn^{total}]$. Figure 5 shows the relationship between the formation ratio of dissolved Zn (II) species and pH value at $[NH_3] = 0.1$ mol l^{-1}, and 1.5 mol l^{-1}. The change in pH range for the formation of Zn-NH_3-complex species depends on $[NH_3]$. At $[NH_3]= 1.5$ mol l^{-1}, the state of Zn dissolved in the aqueous solution presents as Zn^{2+} hydrate ion at a pH value below 5, and the Zn-NH_3 complexes with different NH_3 coordination numbers are formed at higher pH values, resulting in a narrower stable region of $Zn(OH)_2$(s). Although the solution used for the chemical bath deposition (CBD) contained thiourea in addition to Zn salts and NH_3, consideration of Zn-thiourea complex as a dissolved species in aqueous solution is omitted.

Figure 6 shows the potential-pH diagram for the Zn-NH_3-water system at $a_{Zn^{2+}} = 0.05$ mol l^{-1}, $T = 298$ K, and the solubility curves for ZnO, $Zn(OH)_2$, and ZnS at 298 and 353 K. The potential-pH diagram (Fig. 6a) was drawn by considering the reactions among the Zn-NH_3-complex, metallic Zn, and $Zn(OH)_2$(s). The standard electrode potential (E^0) and equilibrium constant (K) related to the oxidation-reduction and acid-base reactions were calculated from the standard reaction Gibbs energy ($\Delta_r G^0$) in the same manner as described in the previous section. For example, the calculation to estimate the critical pH value of the higher pH side of the $[Zn(NH_3)_4]^{2+}$ stable region is as follows:

$$Zn(NH_3)_4^{2+} + 2H_2O \rightleftharpoons Zn(OH)_2(s) + 2H^+ + 4NH_3$$

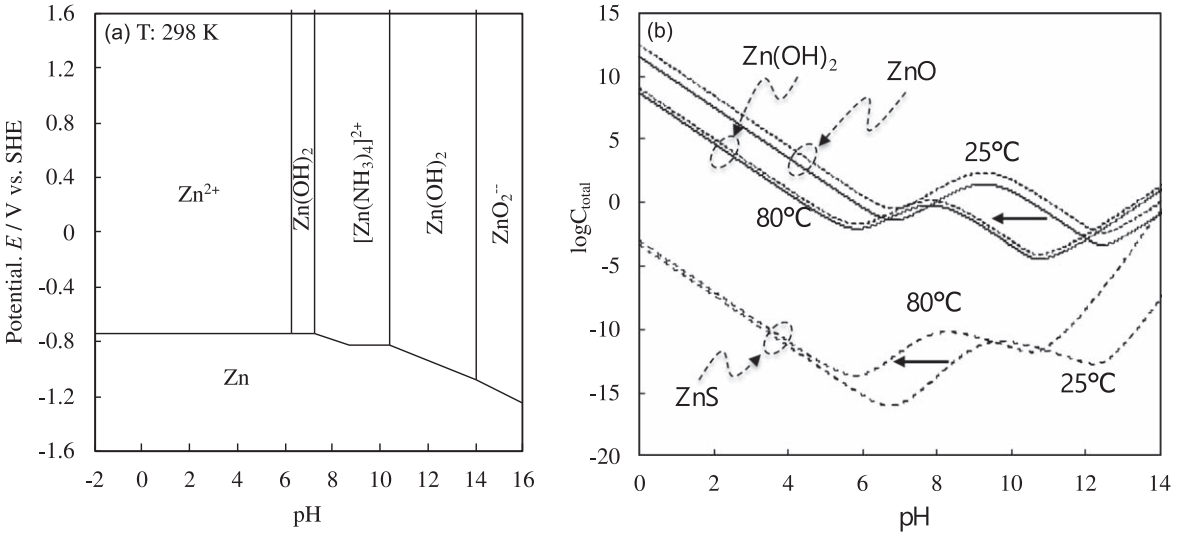

Figure 6 . Potential-pH diagram(a) and solubility curve (b) of ZnO, $Zn(OH)_2$, and ZnS at 298 K and 353 K for the Zn-NH_3-water system. $[Zn^{2+}] = 0.05\ mol\ l^{-1}$, $[NH_3] = 1.5\ mol\ l^{-1}$.

$$\log_{10}[Zn(NH_3)_4^{2+}] + \log_{10} K = 4\log_{10}[NH_3] - 2pH$$

$$\Delta_r G^0 = \{(\mu^o_{Zn(OH)_2} + 4\mu^o_{NH_3}) - (\mu^o_{Zn(NH_3)_4^{2+}} + 2\mu^o_{H_2O})\} = -RT\log_e K$$

$$\log_{10} K = -20.49$$

Then, roughly assuming that $[Zn(NH_3)_4^{2+}] = 0.1\ mol\ l^{-1}$, $[NH_3] = 1\ mol\ l^{-1}$, the upper critical pH value is calculated to be 10.75. The stable region of dissolved Zn-NH_3 complex species appears at around pH = 9 and is sandwiched between two split regions of $Zn(OH)_2$(s) and borders the metallic Zn region at the bottom. As such, changes in the equilibrium electrode potentials and equilibrium pH values depend on the concentrations of the Zn ions and NH_3.

The calculated solubility curves of ZnO and ZnS are shown in Fig. 6b in addition to that of $Zn(OH)_2$. The effects of temperature on the profile of the potential-pH diagram and solubility curves can be estimated from the standard reaction Gibbs energy ($\Delta_r G_T{}^0$), standard enthalpy($\Delta_r H_T{}^0$), standard entropy($\Delta_r S_T{}^0$), and standard heat capacity($\Delta C_p{}^0$) by using the following equation:

$$\Delta_r G_T^0 = \Delta_r H_T^0 - T\Delta_r S_T^0 = \left[\Delta_r H^0_{298.15} + \int_{298.15}^{T} \Delta C_p^0 dT\right] + T\left[\Delta_r S^0_{298.15} + \int_{298.15}^{T} (\Delta C_p^0/T) dT\right]$$

The profiles of the solubility curves for ZnO and $Zn(OH)_2$ in the Zn-NH_3-water system are distinctly different to those for Zn-water system shown in Fig. 2b. The solubilities of ZnO, $Zn(OH)_2$, and ZnS in the Zn-NH_3-water system showed a local maximum at around pH = 10 with the formation of the $Zn(NH_3)_4{}^{2+}$ complex at 298 K, which decreases with the increase or decrease in pH value. The solubility of ZnS is much less than those for ZnO and $Zn(OH)_2$, and all the solubility curves shifted to the lower pH side by increasing the temperature of the solution.

The Zn(S,O,OH) buffer layers used for Cu(In,Ga)Se_2 solar cells have been prepared by the chemical bath deposition (CBD) process, which depositions are carried out by raising the solution temperature after immersing the substrate into the CBD solution (pH = ~10)

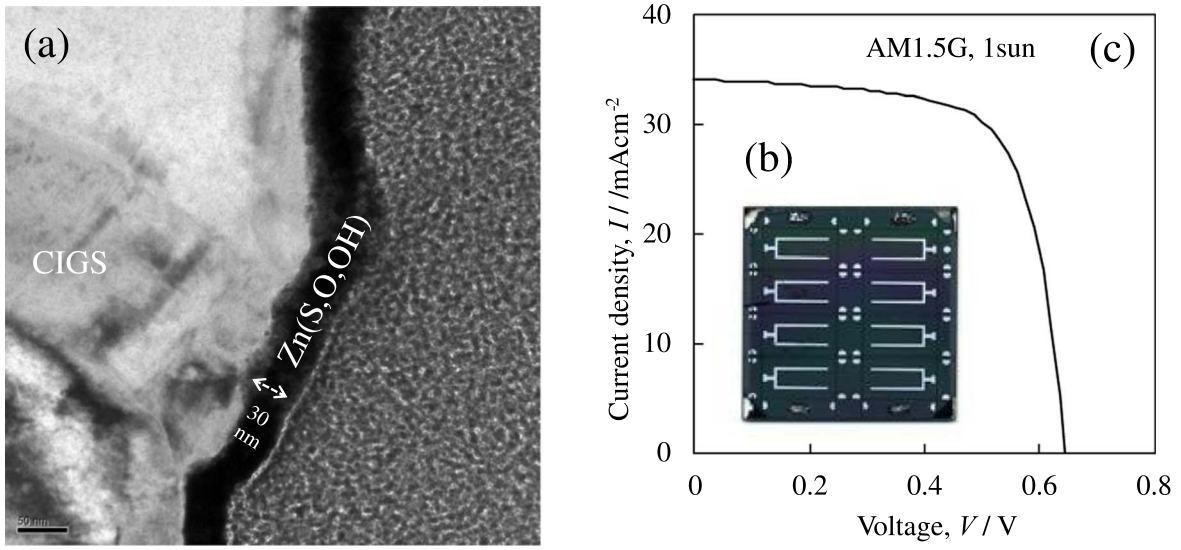

Figure 7. Transmission electron microscopy image of the cross-section (a), appearance (b), and performance (c) for the 15.5%-efficiency-CIGS solar cell (n-ZnO/ Zn(S,O,OH)/Cu(In,Ga)Se_2/Mo/Glass).

containing zinc salts ($[Zn^{2+}] = 0.05\ mol\ l^{-1}$), thiourea, and ammonia at low temperature of 298 K. The initial state is below the solubility curve of ZnO and $Zn(OH)_2$, and since there is barely any sulfur in the aqueous solution, no precipitation occurs. As the temperature rises, the decomposition of thiourea proceeds on the substrate surface, and sulfur as ZnS is precipitated through a supersaturated state due its extremely low solubility. When the temperature rises to around 353 K, the state of the aqueous solution progresses above the dissolution curve of ZnO and $Zn(OH)_2$ as the curves shifts, resulting in the co-precipitation of ZnO and $Zn(OH)_2$ in addition to ZnS. Thus, it can be predicted from the change in the supersaturation condition that the Zn(S,O,OH) layer prepared by the CBD process is composed of the ZnS-rich layer deposited at low temperature in the initial stage while ZnO, $Zn(OH)_2$-rich layer is deposited at elevated temperatures. In fact, Transmission Electron Microscopy (TEM) and X-ray Absorption Fine Structure (XAFS) analyses indicated that the crystal structure of the Zn(S,O,OH) layer near the $Cu(In,Ga)Se_2$ layer was similar to that of ZnS, and the contents of ZnO, and $Zn(OH)_2$ increased with increase in thickness.[91]

Figure 7 shows the cross-sectional transmission electron microscopy (TEM) image, appearance, and current density-voltage curve under AM1.5 G illumination for the $Cu(In,Ga)Se_2$ solar cell installed a Zn(S,O,OH) buffer layer. The $Cu(In,Ga)Se_2$ solar cell possessed a layered structure of Mo/$Cu(In,Ga)Se_2$/Zn(S,O,OH)/i-ZnO/Ga:ZnO on a soda-lime glass substrate, and the electrons excited in the $Cu(In,Ga)Se_2$ layer by light irradiation transferred down to the n-ZnO layer through the Zn(S,O,OH) buffer layer. The conduction band-offsets were estimated to be over 1 eV for the $Zn(OH)_2$-rich Zn(S,O,OH) layer and 0.5 eV for the ZnS-rich Zn(S,O,OH) layer at the interface to the $Cu(In,Ga)Se_2$ layer. Both the ZnO and $Zn(OH)_2$ layers could be dissolved by immersing in an NH_3 aqueous solution, which the ZnS layer remained, due to the large difference in solubility between ZnS and ZnO($Zn(OH)_2$). The conversion efficiency of the $Cu(In,Ga)Se_2$ solar cell was estimated to be 6.7% for the Zn(S,O,OH) buffer layer composed of ZnS, ZnO, and $Zn(OH)_2$. However, by dissolving the $Zn(OH)_2$-rich Zn(S,O,OH) layer, the $Cu(In,Ga)Se_2$ solar cell with the ZnS-rich Zn(S,O,OH) buffer layer showed an improved conversion efficiency of 15.5%.[92]

Thermodynamic design of electrochemical process for fabricating CuO-Cu_2O bilayers in a single aqueous solution.—P-type semiconducting copper oxides of CuO and Cu_2O with the bandgap energies of 1.5 eV and 2.1 eV, respectively are widely applied as photovoltaic layers in solar cells and photocathodes in the photoelectrochemical water splitting to generate hydrogen gas.[93–103] Cu electroplating have been performed by using copper-sulfate, copper-cyanide complex, and copper-pyrophosphate aqueous solutions, while copper-lactate complex solution has been used for the electrodeposition of Cu_2O layers,[104] due to the difficulty to prepare a simple copper aqueous solution. Additionally, copper-ammonia complex,[17] copper-tartrate complex,[105] and copper-aminoacetate complex solutions[106] have been used for the electrodepositions of the CuO layers, and we have reported a direct electrodeposition of both Cu_2O and CuO layers by switching potentials between anodic and cathodic in the copper-tartrate complex aqueous solution.[107]

Figure 8 shows the potential-pH diagrams for Cu-water, Cu-NH_3-water, and Cu-lactic acid-water systems which were drawn by Izaki, et al.[17] and Murase et al.[108,109] Metallic Cu layer can be prepared by shifting the electrode potential towards a region more negative than the equilibrium electrode potential for the Cu^{2+}/Cu^0 reaction in a copper sulfate aqueous solution. This would correspond to the shift of potential from the Cu^{2+} region downwards to the metallic Cu region in the Cu-water potential-pH diagram (Fig. 8a). The CuO region is located at higher pH values compared to the Cu^{2+} region, while the Cu_2O region is sandwiched between the CuO and metallic Cu regions. A diagonal line for the Cu^{2+}/Cu_2O reaction is represented in the diagram as the reduction reaction from Cu^{2+} to Cu^{1+} states. At pH values below 3, the Cu^{2+} ion is reduced directly to metallic Cu at $[Cu^{2+}] = 1\ mol\ l^{-1}$, where the region does not border with Cu_2O(s). The Cu^{2+} ion is reduced to metal Cu through Cu^{1+} states at pH value over 3, where there is a window of possibility for the direct preparation of the Cu_2O layer in a simple Cu aqueous solution. In fact, particulate Cu_2O has been directly electrodeposited on a substrate by using a cathodic reaction in a simple copper nitrate aqueous solution at pH 3.8∼5.1,[110] but preparation of a compact and continuous p-Cu_2O layer remains a challenge by this method. As aforementioned, the CuO region is located at a higher pH value compared to the Cu^{2+} region, thus raising the pH value in the vicinity of the substrate is necessary to prepare a CuO layer. However, the nitrate reduction reaction strategy cannot be applied to the CuO electrodeposition, due to the negative equilibrium electrode potential of the nitrate reduction reaction compared to that of the Cu^{2+}/Cu^0 reduction reaction. On the other hand, the potential shift by anodic polarization can result in a decrease in pH value due to the oxygen generation reaction as shown by the red dotted line in Fig. 8b, rendering the direct preparation of the CuO layer impossible. To address this, the Cu-complex aqueous solutions were developed to achieve direct electrodeposition of Cu_2O and CuO layers. Figure 8b shows the potential-pH diagram thermodynamically drawn for the Cu-NH_3-water system, and the reaction in the Cu-NH_3-water system are as follows:

$$Cu^{2+} + H_2O \rightleftarrows CuO + 2H^+: \log_{10} K = -7.35$$

$$CuO + H_2O \rightleftarrows Cu(OH)_2: \log_{10} K = -1.74$$

$$Cu^{2+} + NH_3 \rightleftarrows Cu(NH_3)^{2+}: \log_{10} K = 4.28$$

$$Cu(OH)_2 + NH_3 + 2H^+ \rightleftarrows Cu(NH_3)^{2+} + 2H_2O: \log_{10} K = 4.28$$

$$Cu(NH_3)^{2+} + NH_3 \rightleftarrows Cu(NH_3)_2^{2+}: \log_{10} K = 3.56$$

$$Cu(NH_3)_2^{2+} + NH_3 \rightleftarrows Cu(NH_3)_3^{2+}: \log_{10} K = 2.90$$

$$Cu(NH_3)_3^{2+} + NH_3 \rightleftarrows Cu(NH_3)_4^{2+}: \log_{10} K = 2.18$$

$$CuO + NH_3 + 2H^+ \rightleftarrows Cu(NH_3)_2^{+}: \log_{10} K = 11.6$$

$$2Cu^{2+} + H_2O + 2e \rightleftarrows Cu_2O + 2H^+: E^0 = 0.207\ V\ vs\ SHE$$

$$Cu_2O + 4NH_4^+ \rightleftarrows 2Cu(NH_3)_2^+ + H_2O + 2H^+: \log_{10} K = -17.39$$

$$Cu_2O + 4NH_3 + 2H^+ \rightleftarrows 2Cu(NH_3)_2^+ + H_2O: \log_{10} K = 19.61$$

By considering the above reactions, stable regions of dissolved $Cu^{I}(NH_3)_2^+$ and $Cu^{II}(NH_3)_4^{2+}$complexes could be drawn within the CuO and Cu_2O regions in the potential-pH diagram as shown in Fig. 8b, which do not exist in the potential-pH diagram of a simple Cu-water system. Also as shown, the metal Cu region is located under the Cu-NH_3 complex region at lower potentials, and the Cu-NH_3 complexes regions appear sandwiched between regions of split Cu_2O and CuO. As such, metal Cu layer can be electrochemically deposited from the Cu-NH_3 complex region by cathodic polarization with the absence of the Cu_2O underneath. On the other hand, anodic polarization at a potential above the oxygen generation reaction can decrease the local pH value in the vicinity of the substrate, making the electrodeposition of CuO layer possible, as shown with the dotted arrow. The reactions can be expressed as follows:

$$2H_2O \rightleftarrows O_2 + 4H^+ + 4e^-$$

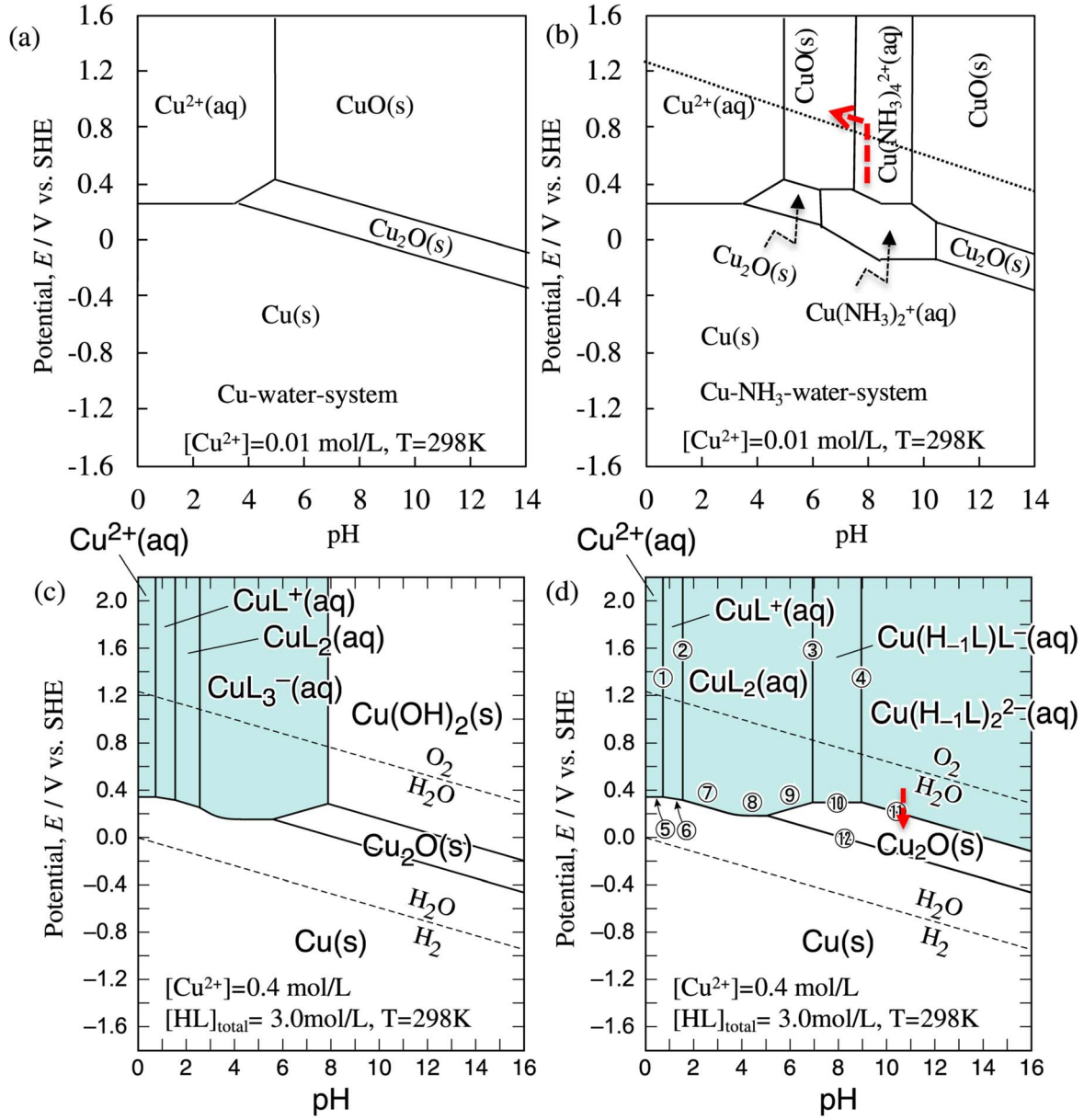

Figure 8. Potential-pH diagrams for Cu-water (a), Cu-NH_3-water (b), and Cu-lactic acid-water systems (c), (d).

$$Cu(NH_3)_4^{2+} + 4H^+ \rightarrow Cu^{2+} + 4NH_4^+$$

$$Cu^{2+} + 2OH^- \rightarrow Cu(OH)_2$$

$$Cu(OH)_2 \rightarrow CuO + H_2O$$

The p-CuO layer prepared by this method can function as photocathodes in photoelectrochemical water splitting and photovoltaic layers in solar cells when coupled with n-ZnO layers.

The direct electrodeposition of a p-Cu_2O layer by cathodic polarization in a Cu-lactate complex aqueous solution was reported by Rakhashani in 1986.[104] Aqueous solution containing 0.4 mol l^{-1} copper salt and 3 mol l^{-1} lactic acid at around pH 9.0–12.5. has been used generally for the Cu_2O electrodeposition since.[19] Also, heating metal Cu in air and various sputtering techniques have been used for the preparation of Cu_2O layer, but the thermodynamically stable phase at room temperature at 1 atmospheric pressure is CuO, not Cu_2O. The Cu_2O layer have been prepared by heating Cu sheets at 1273K–1473 K, followed by the removal of the surface CuO layer which is formed during cooling by chemical treatment,[111] to get the Cu_2O single layer function as photovoltaic applications.

In a Cu-lactic acid (HL)-water system, the Cu-lactate complexes and their $\log_{10}K$ values are as follows:

$$HL \rightleftarrows H^+ + L^-: \log_{10}K = -3.81$$

$$Cu^{2+} + L^- \rightleftarrows CuL^+: \log_{10}K = 2.45$$

$$Cu^{2+} + 2\,L^- \rightleftarrows CuL_2: \log_{10}K = 4.08$$

$$Cu^{2+} + 3\,L^- \rightleftarrows CuL_3^-: \log_{10}K = 4.70$$

$$Cu^{2+} + 2OH^- \rightleftarrows Cu(OH)_2: \log_{10}K = 8.81$$

Figure 8c shows the potential-pH diagram drawn on the basis of the above reactions for the aqueous solution containing 0.4 mol l^{-1} Cu salt and 3 mol l^{-1} lactic acid by Murase et al.[109] The stable regions of dissolved Cu^{2+} cation and Cu-lactate complexes exist at pH

values below 8, while the $Cu(OH)_2(s)$ region appears at pH values above 8, according to the known stability constants. However, experimentally prepared aqueous solution containing Cu salt and lactic acid showed an appearance of bright blue in color, which turned dark blue and finally violet when the pH value was increased, without any precipitation forming in the solution, even at a high pH value of 12.5. This suggests the existence of unknown Cu-lactate complexes, which are stable at high pH values. In fact, two Cu-lactate complexes of $Cu(H_{-1}L)L^-$ and $Cu(H_{-1}L)_2{}^{2-}$ were newly identified by Electrospray Ion Mass Spectrometry (ESI-MS) and titration, and the following reactions were suggested.[108,109]

$$CuL_2 + OH^- \rightleftarrows Cu(H_{-1}L)L^- + H_2O$$

$$CuL_2 + 2OH^- \rightleftarrows Cu(H_{-1}L)_2^{2-} + 2H_2O$$

The $\log_{10}K$ values for the identified Cu-lactate complexes were determined by absorption spectra measurements:

$$Cu^{2+} + 2\,L^- \rightleftarrows Cu(H_{-1}L)L^- + H^+ : \log_{10}K = -2.87$$

$$Cu^{2+} + 2\,L^- \rightleftarrows Cu(H_{-1}L)_2^{2-} + 2H^+ : \log_{10}K = -11.82$$

The equilibrium reactions and the equilibrium equations based on the above findings for the Cu lactate acid solution are shown as follows:

$$Cu^{2+} + HL \rightleftharpoons CuL^+ + H^+ : pH = 1.36 + \log_{10}([CuL^+]/[Cu^{2+}]) - \log_{10}[HL]$$

$$CuL^+ + HL \rightleftharpoons CuL_2 + H^+ : pH = 2.18 + \log_{10}([CuL_2]/[CuL^+]) - \log_{10}[HL]$$

$$CuL_2 \rightleftharpoons Cu(H_{-1}L)L^- + H^+ : pH = 6.95 + \log_{10}([Cu(H_{-1}L)L^-]/[CuL_2])$$

$$Cu(H_{-1}L)L^- \rightleftharpoons Cu(H_{-1}L)_2^{2-} + H^+ : pH = 8.95 + \log_{10}([Cu(H_{-1}L)_2^{2-}]/[Cu(H_{-1}L)^-])$$

$$Cu^{2+} + 2e^- \rightleftharpoons Cu : E = 0.337 + 0.0295\log_{10}[Cu^{2+}](V \text{ vs SHE})$$

$$CuL^+ + H^+ + 2e^- \rightleftharpoons Cu + HL : E = 0.377 + 0.0295(\log_{10}[CuL^+] - \log_{10}[HL] - pH)(V \text{ vs SHE})$$

$$CuL_2 + 2H^+ + 2e^- \rightleftharpoons Cu + 2HL : E = 0.441 + 0.0295(\log_{10}[CuL_2] - 2\log_{10}[HL] - 2pH)(V \text{vs SHE})$$

$$CuL_2 + 2e^- \rightleftharpoons Cu + 2L^- : E = 0.216 + 0.0295(\log_{10}[CuL_2] - 2\log_{10}[L^-]) \times (V \text{ vs SHE})$$

$$2CuL_2 + H_2O + 2e \rightleftharpoons Cu_2O + 2H^+ + 4L^-$$

$$:E = -0.039 + 0.0591(\log_{10}[CuL_2] - 2\log_{10}[L^-] + pH)(V \text{ vs SHE})$$

$$2Cu(H_{-1}L)L^- + H_2O + 2e^- \rightleftharpoons Cu_2O + 4L^-$$

$$:E = 0.371 + 0.0591(\log_{10}[Cu(H_{-1}L)L^-] - 2\log_{10}[L^-])(V \text{ vs SHE})$$

$$2Cu(H_{-1}L)L_2^{2-} + H_2O + 2H^+ + 2e \rightleftharpoons Cu_2O + 4L^-$$

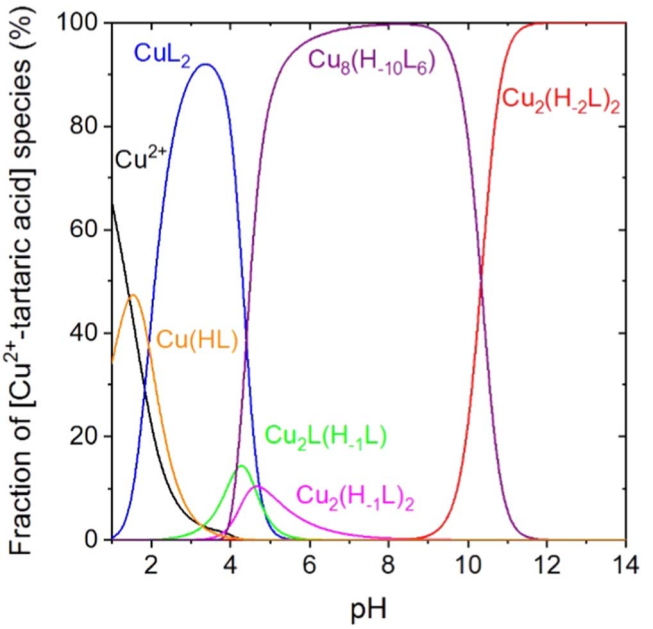

Figure 9. Fraction of dissolved species for the Cu(II)-tartrate complex aqueous solution.

$$:E = 0.903 + 0.0591(\log_{10}[Cu(H_{-1}L)L_2^{2-}] - 2\log_{10}[L^-] - pH)(V \text{ vs SHE})$$

$$Cu_2O + 2H^+ + 2e^- \rightleftharpoons 2Cu + H_2O$$

$$:E = 0.903 + 0.0591(\log_{10}[Cu(H_{-1}L)L_2^{2-}] - 2\log_{10}[L^-] - pH)(V \text{ vs SHE})$$

The potential-pH diagram for the Cu-lactate complex solution drawn according to the above reactions and equations is shown in Fig. 8d, where even at pH values higher than 8, dissolved species of $Cu(H_{-1}L)L^-(aq)$ and $Cu(H_{-1}L)_2{}^{2-}(aq)$ are considered. At pH 12.5, the Cu_2O region is located at the bottom of the Cu-lactate complex region, and the diagram shows consistency with the experimental result.

As already been reported, Cu_2O and CuO can both act as photovoltaic layers, and it is favorable to include several p-type semiconductors with different bandgap energies in a photovoltaic layer to realize a high conversion efficiency, as demonstrated in a multijunction solar cell composed of InGaP, InGaAs, and Ge cells with a conversion efficiency over 30%.[112] Also, research works on the CuO/Cu_2O bilayer photocathodes for applications in photoelectrochemical water splitting to generate hydrogen gas have become active of late. Several techniques involving thermal oxidation have been reported to prepare the CuO/Cu_2O bilayers, but defects such as nanopores and lattice defects induced during the heating process can pose negative effects to the photovoltaic properties including carrier generation and transportation.[113]

As aforementioned, in a Cu-lactate complex solution, a Cu_2O layer can be deposited by cathodic polarization at pH values ranging from 9 to 12.5, but a CuO layer cannot be deposited. In contrast, in a Cu-NH_3 complex solution, a CuO layer can be deposited by anodic polarization, but not the Cu_2O layer. However, from the above investigation on Cu-complexes, if there exist a system where the CuO region is bordered at pH values lower or higher than the Cu-complex region like the Cu-NH_3 aqueous solution, and at the same time possesses a Cu_2O region located at the bottom of the Cu-complex region in the lower potential area like the Cu-lactic acid aqueous solution, such aqueous solution will give the formation of both Cu_2O and CuO layers by merely controlling the deposition potential in that same aqueous solution. And since the equilibrium

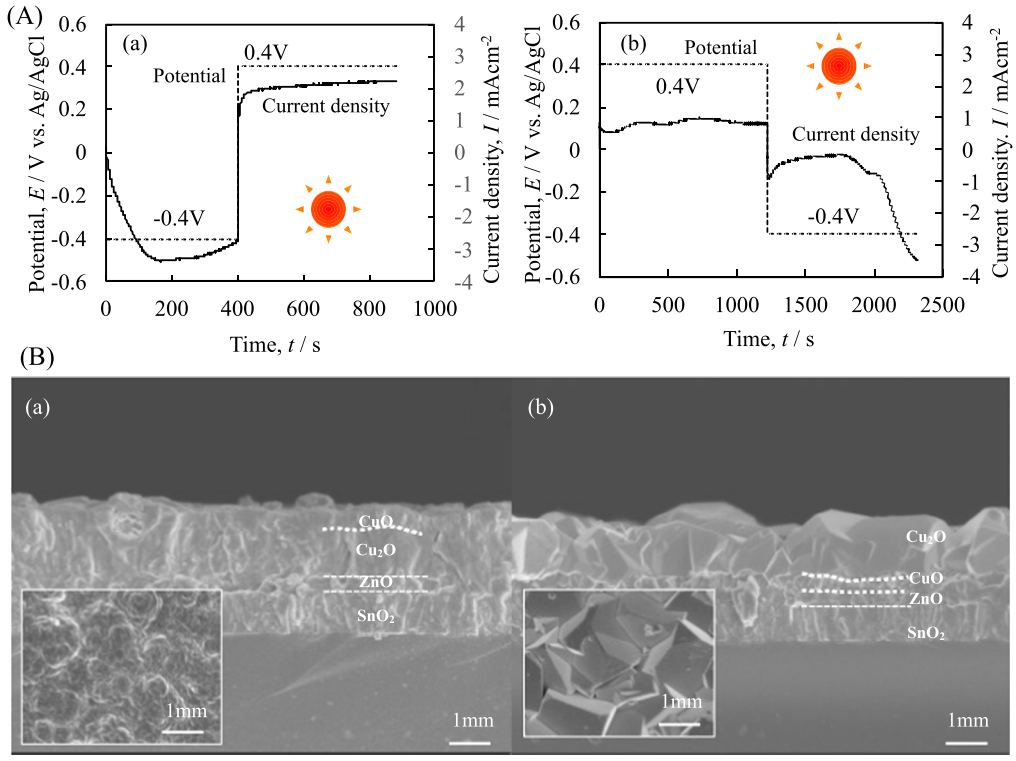

Figure 10. Chronoamperometry curves (A) and FE-SEM images (B) for CuO/Cu_2O (a) and Cu_2O/CuO bi-layers (b) prepared by cathodic/anodic polarization switching under light irradiation.

pH value for the formation of CuO and equilibrium electrode potential for Cu_2O are functions of the stability constant of the Cu-NH_3 and Cu-lactate complexes, this means that it is possible to prepare both Cu_2O and CuO layers in an aqueous solution containing a ligand with the appropriate stability constant. Based on these criteria, tartaric acid was selected as the appropriate ligand. Figure 9 shows the pH dependence of the dissolved chemical species for the Cu-tartaric acid (H_2L = HCOOCCH(OH)CH(OH)COOH) solution. The Cu^{2+} ion is dissolved as $[Cu_2(H_{-2}L)_2]^{4-}$ complex in the aqueous solution in the region of high pH values. As such, a Cu_2O layer can be deposited by cathodic polarization by the following reactions:

$$[Cu_2(H_{-2}L)_2]^{4-} + 2e^- \rightleftarrows 2Cu^+ + 2(H_{-2}L)^{4-}$$

$$Cu^+ + OH^- \rightleftarrows CuOH$$

$$2CuOH \rightleftarrows Cu_2O + H_2O$$

Also in the same solution, a CuO layer can be deposited by anodic polarization at potentials more positive than the oxygen generation reaction as follows:

$$2H_2O \rightleftarrows O_2 + 4H^+ + 4e^-$$

$$[Cu_2(H_{-2}L)_2]^{4-} + 2H^+ \rightleftarrows [Cu_2(H_{-1}L)_2]^{2-}$$

$$[Cu_2(H_{-1}L)_2]^{2-} + 4OH^- \rightleftarrows 2Cu(OH)_2 + 2(H_{-1}L)^{3-}$$

$$Cu(OH)_2 \rightleftarrows CuO + H_2O$$

The Cu_2O and CuO layers prepared by cathodic and anodic polarizations from this Cu-tartaric acid aqueous solution possessed the respective characteristic semiconductor features of a cubic lattice with the bandgap energy of 2.1 eV and a monoclinic lattice with the bandgap energy of 1.5 eV.[106]

Figure 10 shows the chronoamperometry curves and cross-sectional FESEM images for the CuO/Cu_2O bilayers prepared by a light-irradiated potential-switching electrodeposition. The CuO/Cu_2O and Cu_2O/CuO bilayers were prepared by only switching the potential to cathodic and anodic polarization for the respective Cu_2O and CuO electrodeposition in the same Cu-tartrate complex solution. Since holes, which are the majority carriers in the p-Cu_2O layer, are needed for the CuO electrodeposition, CuO/Cu_2O bilayers could be successfully prepared by the potential-switching. On the other hand, since electrons are needed for the electrodeposition of Cu_2O, which unfortunately are the minority carriers in the p-CuO layer, the preparation of Cu_2O/CuO bilayer was predicted to be very difficult in the dark. However, under the irradiation of light, after the formation of the CuO layer, photon energies larger than the bandgap energy of CuO induce the excitation of electrons from the valence band to the conduction band, which are then swept down towards the interface of the solution by an electric field formed at the interface. The electrons reaching the interface will then drive the reactions of the Cu_2O electrodeposition, consequently completing the preparation of Cu_2O/CuO bilayer under light irradiation.

Conclusions

Electrochemical processes in aqueous solutions are widely used as electroplating and electroless plating of metals, alloys, and composites, and the process is being extended to direct preparations of metal oxides and precursors of metal compounds for solar cell applications. The electrochemical process can be understood and designed based on thermodynamics as summarized in various published reviews, and it is widely approved that the soluble chemical species, potential-pH diagram, and solubility curves drawn based on thermodynamics are useful for the understanding and designing the electrochemical process.

In this review, the equilibrium electrode potentials, critical pH values, and dissolved chemical species relating to the oxidation-reduction, acid-base, and ligand-exchanging reactions, which constitute the major reactions in an aqueous solution, and the calculation

of the standard Gibbs free energy were firstly discussed. The change in the equilibrium electrode potential depending on the resultant materials of metal and metal compound was described as demonstrated in the electrochemical preparation of the Cu-In-Se precursor for the $Cu(In,Ga)Se_2$ solar cell application. In addition, the advantages, usefulness and practicality of the soluble chemical species, potential-pH diagrams, and solubility curves were discussed and demonstrated in examples of direct electrodepositions of metal oxides, the chemical introduction of impurities into ZnO to enable characteristics control, the chemical bath deposition process (CBD) for Zn(S,O,OH) buffer layer preparation in $Cu(In,Ga)Se_2$ solar cells, and finally, the design of the electrochemical process for fabricating CuO/Cu_2O bilayers.

As shown in this review, although most thermodynamic data including the chemical potentials and stability constants are readily available for calculations, it is sometimes insufficient in practical uses, as demonstrated in the case of Cu-lactic acid complex. How we make good use of the thermodynamic data and the applications for its calculations are very important in opening new doors to develop novel electrochemical processes and state-of-the-art materials.

Acknowledgments

This work was supported financially by Grants-in-Aid for Scientific Research (B) (No. 19H02810) from the Japan Society for the Promotion of Science (JSPS).

ORCID

Masanobu Izaki https://orcid.org/0000-0002-3959-1923
Tsutomu Shinagawa https://orcid.org/0000-0001-5671-1512

References

1. M. Schlesinger and M. Paunovic, *Modern Electroplating* (Wiley, New York, NY) 5th ed., 383 (2010).
2. W. H. Safranek, *The Properties of Electrodeposited Metals and Alloys* (American Electroplaters and Surface Finishers Society, Orland) 2nd ed. (1986).
3. D. Lincot, *Thin Solid Films*, **487**, 40 (2005).
4. J. A. Switzer, *Am. Ceram. Soc. Bull.*, **66**, 1521 (1987).
5. T. P. Niesen and M. R. De Guire, *Solid State Ionics*, **151**, 61 (2002).
6. D. Tench and L. F. Warren, *J. Electrochem. Soc.*, **130**, 869 (1983).
7. D. Elwell and R. S. Feigelson, *Sol. Energ. Mater.*, **6**, 129 (1982).
8. D. Elwell, *J. Cryst. Growth*, **52**, 741 (1981).
9. R. C. Mattei, D. Elwell, and R. S. Feigelson, *J. Cryst. Growth*, **43**, 643 (1978).
10. K. Uosaki, M. Takahashi, and H. Kita, *Electrochim. Acta*, **29**, 279 (1984).
11. C. Lepiller and D. Lincot, *J. Electrochem. Soc.*, **151**, C348 (2004).
12. J. A. Switzer, *J. Electrochem. Soc.*, **133**, 722 (1986).
13. M. Izaki and T. Omi, *Appl. Phys. Lett.*, **68**, 2439 (1996).
14. S. Peulon and D. Lincot, *Adv. Mater.*, **2**, 166 (1996).
15. J. Rousset, F. Tsin, M. Guc, J. Videl, A. Le Bris, A. Thomere, V. Izquierdo-Roca, and D. Lincot, *J. Phys. Chem. C*, **120**, 18953 (2016).
16. J. A. Switzer, H. M. kothari, P. Poizot, S. Nakanishi, and B. W. Bohanan, *Nature*, **425**, 490 (2003).
17. M. Izaki, M. Nagai, K. Maeda, F. B. Mohamad, K. Motomura, J. Sasano, T. Shinagawa, and S. Watase, *J. Electrochem. Soc.*, **158**, D578 (2011).
18. K. Nakaoka and K. Ogura, *J. Electrochem. Soc.*, **149**, C579 (2002).
19. T. D. Golden, M. G. Shumsky, Y. Zhou, R. A. VanderWelf, R. A. Van Leeuwen, and J. A. Switzer, *Chem. Mater.*, **8**, 2499 (1996).
20. K. Mizuno, M. Izaki, K. Murase, T. Shinagawa, M. Chigane, M. Inaba, A. Tasaka, and Y. Awakura, *J. Electrochem. Soc.*, **152**, C179 (2005).
21. G. M. McShane and K.-S. Choi, *J. Am. Chem. Soc.*, **131**, 2561 (2009).
22. M. J. Siegfied and K.-S. Choi, *Adv. Mater.*, **16**, 1743 (2004).
23. M. Izaki, T. Saito, M. Chigane, M. Ishikawa, J. Katayama, M. Inoue, and M. Yamashita, *J. Mater. Chem.*, **11**, 1972 (2001).
24. F. B. Li and G. E. Thompson, *J. Electrochem. Soc.*, **146**, 1809 (1999).
25. A. J. Aldykiewicz, A. J. davenport, and H. S. Isacca, *J. Electrochem. Soc.*, **143**, 147 (1996).
26. Y. Zhou and J. A. Switzer, *J. Am. Ceram. Soc.*, **78**, 981 (1995).
27. M. Izaki, *Electrochem. Solid-State Lett.*, **1**, 215 (1998).
28. T. A. Sorenson, S. A. Morton, G. D. Waddeill, and J. A. Switzer, *J. Am. Chem. Soc.*, **124**, 7604 (2002).
29. M. Izaki and O. Shinoura, *Adv. Mater.*, **13**, 142 (2001).
30. M. Abe and Y. Tamura, *J. Appl. Phys.*, **55**, 26148 (1984).
31. T. Itoh, S. Hori, M. Abe, and Y. Tamura, *J. Appl. Phys.*, **69**, 5911 (1981).
32. R. Schrebler, K. Bello, F. vera, P. Cury, E. Munoz, R. del Rin, H. G. Meier, R. Cordova, and E. A. Dulchiede, *Electrochem. Solid State Lett.*, **9**, C130 (2006).
33. B. E. Beyfogle, C.-J. Hung, M. G. Shumsky, and J. A. Switzer, *J. Electrochem. Soc.*, **143**, 2741 (1996).
34. Y. Ida, S. Watase, T. Shinagawa, M. Watanabe, M. Chigane, M. Inaba, A. Tasaka, and M. Izaki, *Chem. Mater.*, **20**, 1254 (2008).
35. D. Lincot et al., *Sol. Energy*, **77**, 725 (2004).
36. S. Ahmed, K. B. Reuter, O. Gunawan, L. Guo, L. T. Romankiw, and H. Deligiani, *Adv. Energy Mater.*, **2**, 253 (2012).
37. K. Murase, H. Uchida, T. Hirato, and Y. Awakura, *J. Electrochem. Soc.*, **146**, 531 (1999).
38. F. Xiao, C. Hangarter, B. Yoo, Y. Rheem, K.-H. Lee, and N. V. Myung, *Electrochem. Acta*, **53**, 8103 (2008).
39. H. Nagayama, H. Honda, and H. Kawahara, *J. Electrochem. Soc.*, **135**, 2013 (1988).
40. H. Kishimoto, K. Takahama, N. Hashimoto, Y. Aoi, and S. Deki, *J. Mater. Chem.*, **8**, 2019 (1998).
41. S. Deki, Y. Aoi, O. Hiroi, and A. Kajinami, *Chem. Lett.*, **25**, 433 (1996).
42. D. Lincot and R. O. Borges, *J. Electrochem. Soc.*, **139**, 1880 (1992).
43. R. O. Borges and D. Lincot, *J. Electrochem. Soc.*, **140**, 3464 (1993).
44. C. Hubert, N. Naghavi, O. Roussel, A. Echeberry, D. Hariskos, R. Menner, M. Powalla, O. Kerrec, and D. Lincot, *, Prog. Photovol.: Res. Appl.*, **17**, 470 (2009).
45. G. Hodes, *Chemical Solution Deposition of Semiconductor Films* (Marcell Dekker, New York, NY) 1 (2003).
46. R. I. Walton, *Chemistry-A European Journal*, **26**, 9041 (2020).
47. G. Demazeau, *J. Mater. Sci.*, **43**, 2104 (2008).
48. M. Yoshimura and K. Byrappa, *J. Mater. Sci.*, **43**, 2085 (2008).
49. M. Paunovic and M. Schlesinger, *Fundamentals of Electrochemical Deposition* (Wiley, NewYork, NY) 51 (1998).
50. P. Delahay, M. Pourbaix, and P. van Rysselberghe, *J. Chem. Edu.*, **27**, 683 (1950).
51. D. W. Barnum, *J. Chem. Edu.*, **59**, 809 (1982).
52. M. Pourbaix, *Atlas of Electrochemical Equilibria* (National Association of Corrosion Engineers, Texas) 84 (1974).
53. J. G. Speight, *Lange's Handbook of Chemistry* (McGRAW-HILL, New York, NY) 6th ed., 1237 (2005).
54. D. D. Wagman, W. H. Evans, V. B. Parker, R. H. Scumm, I. Halow, S. M. Bailey, K. L. Churney, and R. L. Nuttal, "The NBS table of chemical thermodynamic properties, selected values for inorganic and C_1 and C_2 organic substances in SI units." *J. Phys. Chem. Ref.* (National Bureau of Standards, Washington) (1982).
55. J. G. Speight, *Lange's Handbook of Chemistry* (McGRAW-HILL, New York, NY) 6th ed., 1331 (2005).
56. K. Takei, S. Ichikawa, R. Fukazawa, Y. Suzuki, K. Takeuchi, K. Nakamura, and K. Nakazawa, *Micro Electronics Symposium (MES)*, **2004**, 301 (2004).
57. D. Lincot et al., *Sol. Energ.*, **77**, 725 (2004).
58. C. Hubert, N. Naghavi, B. Canava, A. Etcheberry, and D. Lincot, *Thin Solid Films*, **515**, 6032 (2007).
59. S. Aksu, J. Wang, and B. M. Basol, *Electrochem. Solid-State Lett.*, **12**, D33 (2009).
60. S. Peulon and D. Lincot, *J. Electrochem. Soc.*, **145**, 864 (1998).
61. T. Shinagawa, M. Watanabe, J.-i. Tani, and M. Chigane, *Cryst. Growth Des.*, **17**, 3826 (2017).
62. T. Shinagawa, M. Watanabe, T. Mori, J.-I. Tani, M. Chigane, and M. Izaki, *Inorg. Chem.*, **57**, 13137 (2018).
63. S. J. Ahmadi, M. Hosseinpour, F. Javadi, and R. Tayebee, *Ind. Eng. Chem. Res.*, **52**, 1448 (2013).
64. M. Izaki and T. Omi, *J. Electrochem. Soc.*, **144**, 1949 (1997).
65. M. Izaki, S. Watase, and H. Takahashi, *Adv. Mater.*, **15**, 2000 (2003).
66. M. Izaki, T. Shinagawa, and H. Takahashi, *J. Phys. D*, **39**, 1481 (2006).
67. T. Pauporte and D. Lincot, *Appl. Phys. Lett.*, **75**, 3617 (1999).
68. M. Izaki, J. Komori, K. Shimizu, T. Koyama, and T. Shinagawa, *Phys. Status Solidi A*, **214**, 1600473 (2017).
69. M. Kobayashi, J. Komori, M. Izaki, K. Uesugi, A. Takeuchi, and Y. Suzuki, *Appl. Phys. Lett.*, **106**, 081909 (2015).
70. M. Izaki and T. Omi, *J. Electrochem. Soc.*, **144**, L3 (1997).
71. J. E. A. M. Van Den Meerakker, *J. Appl. Electrochem.*, **11**, 395 (1981).
72. M. Lelental, *J. Electrochem. Soc.*, **120**, 1650 (1973).
73. K. Nishiyama, R. Matsuo, J. Sasano, S. Yokoyama, and M. Izaki, *AIP Advance*, **7**, 035004 (2017).
74. T. Pauporte, *J. Electrochem. Soc.*, **149**, C539 (2002).
75. M. Izaki, T. Ohta, M. Kondo, T. Takahashi, F. B. Mohamad, M. Zamzuri, J. Sasano, T. Shinagawa, and T. Pauporte, *ACS Appl. Mater. Interface*, **5**, 13461 (2014).
76. K. Nishiyama, T. Asakawa, J. Sasno, M. Izaki, and T. Fujinami, *J. Surf. Fin. Soc. Jpn.*, **66**, 320 (2015).
77. J. Rousset, E. Saucedo, and D. Lincot, *Chem. Mater.*, **21**, 534 (2009).
78. I. Mora-Sero, F. Fabregat-Santiago, B. Denier, J. Bisquert, R. Tena-Zaera, J. Elias, and C. Levy-Clemont, *Appl. Phys. Lett.*, **89**, 203117 (2006).
79. M. Izaki and J. Katayama, *J. Electrochem. Soc.*, **147**, 210 (2009).
80. M. Izaki and Y. Saijo, *J. Electrochem. Soc.*, **150**, C73 (2003).
81. T. Shinagawa, M. Izaki, H. Inui, K. Murase, and Y. Awakura, *J. Electrochem. Soc.*, **152**, G736 (2005).
82. T. Shinagawa, M. Izaki, H. Inui, K. Murase, and Y. Awakura, *Chem. Mater.*, **18**, 763 (2006).
83. M. T. S. Nair and P. K. Nair, *Semicond. Sci. Technol.*, **4**, 191 (1989).
84. M. Izaki, Y. Yamane, J. Sasano, T. Shinagawa, and M. Inoue, *Electrochem. Solid State Lett.*, **14**, D30 (2011).
85. W. J. Dressick, C. S. Dulsey, J. H. Georger, G. S. Calabrese, and J. M. Calvert, *J. Electrochem. Soc.*, **141**, 210 (1994).
86. J. M. Dona and J. Herrero, *J. Electrochem. Soc.*, **142**, 764 (1995).

87. R. Bayan, C. Guillein, M. A. Marfinez, M. T. Gutierrez, and J. Herrero, *J. Electrochem. Soc.*, **145**, 2776 (1998).
88. C. Hubert, N. Naghavi, O. Rouset, A. Etcheberry, D. Hariskos, R. Menner, M. Powalla, O. Kerrec, and D. Lincot, *Prog. Photovol. Res. Appl.*, **17**, 470 (2009).
89. R. Ortega-Borges and D. Lincot, *J. Electrochem. Soc.*, **140**, 3464 (1993).
90. E. Martell and R. M. Smith, *Critical Stability Constants* (Plenum Press, New York, NY) 5, 291 (1982).
91. M. Izaki, S. Sugiyama, T. Okamoto, Y. Kusano, T. Maki, H. Komaki, H. Shibata, and S. Niki, *Prog. Photovolt.: Res. Appl.*, **24**, 397 (2016).
92. T. Okamoto, H. Komaki, J. Sasano, S. Niki, and M. Izaki, *Energy Proc.*, **60**, 43 (2014).
93. Monica Lira-Cantu (ed.), *The Future of Semiconductor Oxides in Next-Generation Solar Cells* (Elesevier, Amsterdam) 287 (2018).
94. K. Sivula and R. van de Krol, *Nature Reviews/Materials*, **1**, 1 (2016).
95. I. Sullivan, B. Zoellner, and P. A. Maggard, *Chem. Mater.*, **28**, 5999 (2016).
96. C. Li, J. He, Y. Xiao, Y. Li, and J.-J. Delaunay, *Energy Environ. Sci.*, **13**, 3269 (2020).
97. T. Minami, Y. Nishi, and T. Miyata, *APEX*, **9**, 052301 (2016).
98. M. Izaki, T. Shinagawa, K. Mizuno, Y. Ida, M. Inaba, and A. Tasaka, *J. Phys. D*, **40**, 3326 (2007).
99. T. Shinagawa, M. Onoda, B. M. Fariza, J. Sasano, and M. Izaki, *J. Mater. Chem. A*, **1**, 9182 (2013).
100. P. Wang, X. Zhao, and B. Li, *Opt. Exp.*, **18**, 11271 (2011).
101. R. Bhardwaji, R. Barman, and D. Kaur, *Mater. Lett.*, **185**, 230 (2016).
102. S. Masudy-Panah, R. S. Moakhar, C. S. Chua, A. Kushwara, and G. K. Darapati, *ACS Appl. Mater. Interface*, **9**, 27596 (2017).
103. P. L. Khoo, M. Nagai, M. Watanabe, and M. Izaki, *J. Surf. Fin. Soc. Jpn.*, **69**, 469 (2018).
104. A. E. Rakhashani, *Solid State Electron.*, **29**, 7 (1986).
105. P. Poizot, C.-J. Hung, M. P. Nikiforov, E. W. Bohman, and J. A. Switzer, *Electrocehm. Solid-State Lett.*, **6**, C21 (2003).
106. K. Nakaoka, J. Ueyama, and K. Ogura, *J. Electrochem. Soc.*, **151**, C661 (2004).
107. M. Izaki, T. Koyama, P. L. Khoo, and T. Shinagawa, *ACS OMEGA*, **5**, 683 (2020).
108. T. Chen, A. Kitada, Y. Seki, K. Fukami, D. T. Usmanov, L. C. Chen, K. Hiraoka, and K. Murase, *J. Electrochem. Soc.*, **165**, D444 (2018).
109. T. Chen, A. Kitada, K. Fukami, and K. Murase, *J. Electrochem. Soc.*, **166**, D761 (2019).
110. M. J. Siegfried and K. S. Choi, *Angew. Chem. Int. Ed.*, **44**, 3218 (2005).
111. T. Minami, Y. Nishi, and T. Miyata, *APEX*, **6**, 044101 (2013).
112. M. Yamaguchi, *Sol. Energy Mater. Sol. Cells*, **75**, 261 (2003).
113. M. Izaki, K. Fukazawa, K. Sato, P. L. Khoo, M. Kobayashi, A. Takeuchi, and K. Uesugi, *ACS Appl. Energy Mater.*, **2**, 4833 (2019).